Carbohydrate Polymer Technologies and Applications 9 (2025) 100620

Contents lists available at ScienceDirect

Carbohydrate Polymer Technologies and Applications

journal homepage: www.sciencedirect.com/journal/carbohydrate-polymer-technologies-and-applications

Development and characterisation of integrated wet-spun alginate-*Moringa oleifera* composite fibers for potential water purification

Abimbola Oluwatayo Orisawayi [a,b,*], Krzysztof K. Koziol [a], Sameer S. Rahatekar [a,*]

[a] Composites and Advanced Materials Centre, Faculty of Engineering and Applied Sciences, Cranfield University, Bedfordshire MK43 0AL, UK
[b] Department of Mechanical Engineering, School of Engineering and Engineering Technology Olusegun Agagu University of Science and Technology, (OAUSTECH), Okitipupa, Nigeria

ARTICLE INFO

Keywords:
Sodium alginate
Moringa oleifera
Biodegradable polymers
Wet-spinning
Water treatment
Composite fibre

ABSTRACT

Ensuring access to safe drinking water requires effective materials and technologies to treat contaminated water. In this study, we developed sodium alginate fibre (SAlgF) and their composite fibres functionalised with pulverised *Moringa oleifera* (MoP) at concentrations of 0.5 %, 1 %, 4 %, and 8 % using the wet-spinning technique. Both SAlgF and MoP are biodegradable, offering eco-friendly alternatives to synthetic polymers in line with green manufacturing. The results showed significant improvements in the mechanical properties, with the 1 % MoP composite fibre exhibiting 6 times the strength of pure SAlgF in terms of ultimate tensile strength (UTS) and Young's modulus (YM). X-ray Diffraction (XRD) analysis revealed enhanced fibres interactions, while Fourier Transform Infrared Spectroscopy (FTIR) and Thermogravimetric Analysis (TGA) confirmed the successful incorporation of MoP into the alginate matrix and improved thermal stability. Furthermore, the result obtained from the Scanning Electron Microscopy-Energy Dispersive X-ray Spectroscopy (SEM-EDX) indicated morphological changes and the uptake of heavy metal ions when immersed into solutions containing Cu^{2+}, Ni^{2+}, and Cd^{2+}. These findings demonstrate the potential of MoP-modified composite fibres for sustainable and cost-effective water treatment applications, particularly in developing countries.

1. Introduction

Clean water is essential to living organisms and their environments because it plays a crucial role in their survival and well-being. Water is recognised as a vital national asset that is essential for maintaining life on Earth and ensuring the health and prosperity of every ecosystem in the universe (Vardhan, Kumar & Panda, 2019; Xu et al., 2018). Despite this, a significant portion of the global population continues to lack access to clean water. According to the World Health Organisation (WHO) in the report "Progress on Sanitation and Drinking Water-2015 Update and MDG Assessment", approximately 2.6 billion people of the world's population globally do not have access to clean water since 1990 and about 663 million people still lack access to clean water in 2015 (Vardhan, Kumar, & Panda, 2019). The situation is expected to worsen, with the number of individuals living in water-scarce areas projected to rise to approximately 3.9 billion by 2030 (Xu et al., 2018). One of the challenging issues affecting water bodies is the increasing contamination from heavy metal ions due to industrialisation, which poses a significant threat to human health, aquatic life, and the environment. This growing problem has made the removal of these toxic ions a critical focus of research (Saha & Paul, 2019).

Addressing the challenge of removing heavy metal ions, which include Copper (Cu^{2+}), Cadmium (Cd^{2+}), Nickel (Ni^{2+}), Chromium (Cr^{3+}), Lead (Pb^{2+}), Zinc (Zn^{2+}), Mercury (Hg^{2+}), and Arsenic (As^{3+}), has been incredibly difficult and often requires sophisticated technologies such as adsorption, ion exchanges, membranes, and fibres technologies (Xu et al., 2018). The demands for efficient, sustainable materials as alternatives to existing water treatment technologies materials have necessitated the exploration of innovative, environmentally friendly, and cost-effective materials that can facilitate water contaminant removal (Hublikar, Shilar, Suliphuldevara Mathada, & Ganachari, 2024). Biopolymers and biomaterials are known to become upcoming competitive materials due to their attributes of eco-friendliness and biodegradability and several applications range of applications, such as packaging, agricultural, food industries, medical devices, construction, industrial textile and fashion, pharmaceuticals, aerospace, automotive

* Corresponding author.
E-mail addresses: abimbola.orisawayi@cranfield.ac.uk, ao.orisawayi@oaustech.edu.ng, bimboris_t@yahoo.com (A.O. Orisawayi), S.S.Rahatekar@cranfield.ac.uk (S.S. Rahatekar).

https://doi.org/10.1016/j.carpta.2024.100620

Available online 28 November 2024
2666-8939/© 2024 The Authors. Published by Elsevier Ltd. This is an open access article under the CC BY license (http://creativecommons.org/licenses/by/4.0/).

materials, solutions for water purification, and many others (Behrooznia & Nourmohammadi, 2024; Biswal et al., 2024; G. Mishra & Panda, 2024; Panda, Sadeghi, & Seo, 2022). Unlike synthetic polymers, which pose biodegradation challenges and contribute to global warming, bio-based materials from natural resources are more attractive and sustainable. With this limitation, bio-based materials from natural resources are more attractive and sustainable than their oil-based synthetic counterparts (Luckachan & Pillai, 2011).

Among these biopolymers, alginates have been identified as promising biopolymers from natural resources, widely used for different applications (Ananth et al., 2024; Jadbabaei, Kolahdoozan, Naeimi, & Ebadi-Dehaghani, 2021; Kalyani, Smitha, Sridhar, & Krishnaiah, 2006; Sattariazar, Nejad Ebrahimi, & Arsalani, 2023). Alginate biopolymers are unbranched copolymer-block water-soluble polysaccharides, consisting of the pure basic units composed of of M-block β-D-mannuronic acid and G-block α-L-guluronic acid known as its C-5 epimer with monomers typically linked by β-(1–4) glycosidic bonds (Orisawayi et al., 2024; Pawar & Edgar, 2012; Yang et al., 2022). These polysaccharides can exist in various structural forms, such as mixed (MG-Blocks), reversed (GM-Blocks), or with the individual units block residues interspersed with varying length (MG/GM-Blocks) sequences, with different interchangeable possibilities. Alginate can undergo independent sol/gel transition properties in the presence of divalent and trivalent cations. Calcium chloride ($CaCl_2$) is commonly used to form a special structure with (GG Blocks) particularly to facilitate the formation of a strong, rigid gel structure known as the earlier "egg box" (Dash, Gutti, Behera, & Mishra, 2024). Studies have suggested that alginate contains abundantly hydroxide and carboxyl groups which makes it suitable as a material for the adsorption of heavy metal ion from aqueous solutions. (Benettayeb et al., 2024)

Moringa oleifera (*M. oleifera*), often referred to as the "miracle tree" or "drumstick," is another natural resource with significant potential for water purification applications (Amin, Ariwibowo, Putri, & Kurnia, 2024; Liao et al., 2018). Nowadays, *M. oleifera* has naturalised throughout the tropics, including regions in Africa, Central and South America, and Southeast Asia. *M. Oleifera* has even been imported across Europe for research purposes, making it widely available (Bhatia, Othman, & Ahmad, 2006; Leone et al., 2015). Research has shown that *M. oleifera* seeds are rich in protein and possess active functions known for binding with pollutants, making them suitable as antimicrobial flocculants for the removal of wastewater impurities through electrostatic interactions (Benettayeb et al., 2024). Further studies suggest that the protein can be used as an antimicrobial flocculant for the removal of wastewater impurities through the electrostatic interaction between cationic protein and colloids (Fu et al., 2021; Ortolá et al., 2024). Their coagulating properties make them a potential additive for alginate in water purification applications, presenting a successful promising additive to alginate (Orisawayi et al., 2024). However, only a few studies have explored the combination of *M. oleifera* seed and alginate., Although innovative hybrid alginate-pulverised *M. oleifera* composites have been developed using electrospinning (Orisawayi et al., 2024), simple grafting techniques, these methods often require synthetic polymers or toxic crosslinking agents, raising environmental and health concerns (Benettayeb et al., 2024).

This study presents a novel approach to fabricating integrated wet-spun alginate-*M. oleifera* composite fibres (SAlg-MoF) for advanced water purification applications. By incorporating *M. oleifera* seed powder (MoP) into a sodium alginate fibre matrix (SAlgF) using a wet spinning process with a less toxic crosslinking agent, this research aims to significantly enhance the mechanical and thermal properties of the composite fibres, thereby improving their efficacy in water purification. The novel fibre composition is also expected to prevent the mobilisation of MoP into water after treatment, addressing a significant limitation of using *M. oleifera* for water treatment. The significant improvements in the mechanical and thermal properties of the composite fibres demonstrate their potential for various applications, particularly in water purification, thereby contributing to environmental sustainability and the conservation of natural resources. Furthermore, the novel fibres composition is hypothesised to prevent the leaching of MoP into water post-treatment, effectively addressing previous challenges associated with MoP mobilisation. To achieve this, detailed mechanical characterisation to determine the tensile strength and Young's modulus of the fibres. Advanced techniques were employed to validate the properties of the SAlg-MoF composites XRD was used to confirm structural integrity, FTIR to analyse chemical bonding, TGA to determine the thermal stability and SEM-EDX was used to observe morphological changes and elemental interactions within the composites both before and after the adsorption processes. These analyses collectively demonstrated the feasibility of the application of the new SAlg-MoF composites exhibit significantly potential for heavy metal ion adsorption, supporting their suitability for sustainable and biosorbent water purification applications.

2. Materials and methods

2.1. Materials

Sodium alginate (alginic acid sodium salt) from brown algae (SAlgP), with a viscosity of 5.0–40.0 cps $c = 1$ %, (Orisawayi et al., 2024), loss on Drying ≤15.5 %, (c = 1 %, Water @ 25 °C) and weight-average molecular weight ($\overline{M}_w$) is 161 g/mol. The ratio of M:(β-d-mannuronic acid to G:(α-l-guluronic acid) (M/G) is 1.61 (Jafari et al., 2022; Jiang et al., 2023). Product number (Prod. No.): W201502, CAS-Number (CAS):9005–38–3, The product specifications are detailed in N SAlgP was procured from Sigma-Aldrich, UK. *M. Oleifera* seeds were obtained locally through a trusted supplier from Purely Agro Ltd, "DGT"d 2, London, UK. Calcium chloride ($CaCl_2$) (Anhydrous, granular, ≤7.0 mm, ≥93.0 %, d:2.15 g/cm^3, China), Prod. No.:244066, CAS: 10043-52-4. The product specifications are detailed in Table S2. This was obtained from Sigma-Aldrich, China (Orisawayi et al., 2024). Copper (II) acetate monohydrate ($C_4H_6CuO_4 \cdot H_2O$, ≤ 100 %) concentration, Molecular weight (M_w):199.65 g/mol, Prod. No.: 217557, CAS: 6046-93-1, Cadmium acetate dihydrate ($C_4H_6CdO_4 \cdot 2H_2O$), ≤ 100 %, concentration, (M_w): 266.53 g/mol, Prod. No.: 289159, CAS-No.: 5743-04-4,), Nickel (II) acetate tetrahydrate ($C_4H_6CdO_4 \cdot 2H_2O$), ≤ 100 %, concentration) Prod. No. 244066, (M_w):248.84 g/mol CAS: 6018-89-9 These acetate salts were procured from Sigma-Aldrich, UK, and high-purity deionised water supplied by the university laboratory's trusted chemical supplier. (All the listed chemicals were used without further purification)

2.2. Methods

2.2.1. Preparation of MoP

The preparation of the Mop was adopted based on the procedure reported previously (Orisawayi et al., 2024). Briefly, the *M. oleifera* seed was decorticated by separating the seed from the shells and was removed manually to obtain the seeds. The samples were then dried in the vacuum oven for 24 hours at a temperature of 65 °C to reduce the moisture content. The dried samples were preserved in a desiccator in the laboratory until when needed. Pulverisation of the seed samples into grounded fine powder was done using a high-speed PULVERISETTE 14 instrument and milled for about 4–5 min at speeds ranging from 6000 to 10,000 rpm, using a sieve mesh ring or cassette of 2 mm to form the MoP. The MoP was then Stirred with deionised water in different concentrations of 0.5 %, 1 %, 4 %, and 8 %, and stirred continuously for 24 h to ensure homogeneity before use.

2.2.2. Preparation of SAlgP, and SAlgP-MoF solution

Solution of 8 % wt pure SAlgP was prepared for wet-spinning to develop pure SAlgF, Subsequent preparations were prepared separately with fixed 8 % wt. and aqueous suspensions with different

concentrations MoP (0.5 %, 1 %, 4 %, and 8 %) stir constantly for 3 hours were used to develop the SAlg-MoF. Before the wet-spinning process, the resulting solution was loaded into the syringe and kept for 24 hours to remove any air bubbles from the solution before the wet-spinning process.

2.2.3. *Wet spinning process of the fibres*

Fig. 1 shows the simple schematic illustration of the traditional wet-spinning process of the Pure SAlgF and SAlg-MoF of different concentrations. The setup consists of a single syringe pump (Chemyx from Analytical Ltd Sandbach, Cheshire UK), a coagulation bath filled with freshly prepared 4 % wt, $CaCl_2$ solution of about 2 litres for the cross-linking process of SAlgF and SAlg-MoF fibres of different concentrations. A cylindrical rotary collector drum wrapped with aluminium foil was used to collect the fibre. During the wet spinning process, the parameters were kept constant to compare pure SalgF and the different concentrations loaded with MoP (Salg-MoF). The wet spinning process was conducted with the flow rate parameter of 1.0–1.2 uL/h, and a collector speed of 16 rpm. Using a 920050-TE Dispensing Tip (20 Gauge, 12.7 mm length), 0.5 mm inner diameter, with the dispensing tip of a stainless-steel cannula, pink, length of 12.7 mm needle. After the wet spinning process the resulting fibre, were collected and post-treated by soaking it in deionised water for 10 min He et al., (2012) further rinsed several times, and then dried for days before characterisation, The samples were placed in a Gallen Kamp TH 340 L/−40 °C environmental chamber to maintain controlled temperature and humidity conditions. The temperature was regulated within the range of 21 °C to 25 °C, with relative humidity maintained at 45 % over 24 h. These environmental conditions were crucial for ensuring the constant weight of the fibre samples in Fig. 1 (Dos Santos Paglione et al., 2019; He et al., 2012; Hurtado et al., 2022).

2.2.4. *Preparation of heavy metal ion solutions*

For the selective adsorption experiments, a combination of heavy metal ion solutions was prepared, Copper (Cu^{2+}), Cadmium (Cd^{2+}), and Nickel (Ni^{2+}) at a concentration of 50 mg/L each in the same solution. This solution was formulated using precise amounts of salts of copper (II) acetate, nickel (II) acetate, and cadmium (II) acetate to achieve these concentrations in a single 100 mL solution. The stock solutions resulted in aqueous solutions containing 50 mg/l of each of the three heavy metals, Cu^{2+}, Cd^{2+}, and Ni^{2+}. The selection of these salts was confirmed by previous studies (Celebioglu, Topuz, Irem Yildiz, & Uyar, 2019), which highlighted their effective use in similar studies. We have adopted this method to enable the evaluation of preliminary adsorption studies

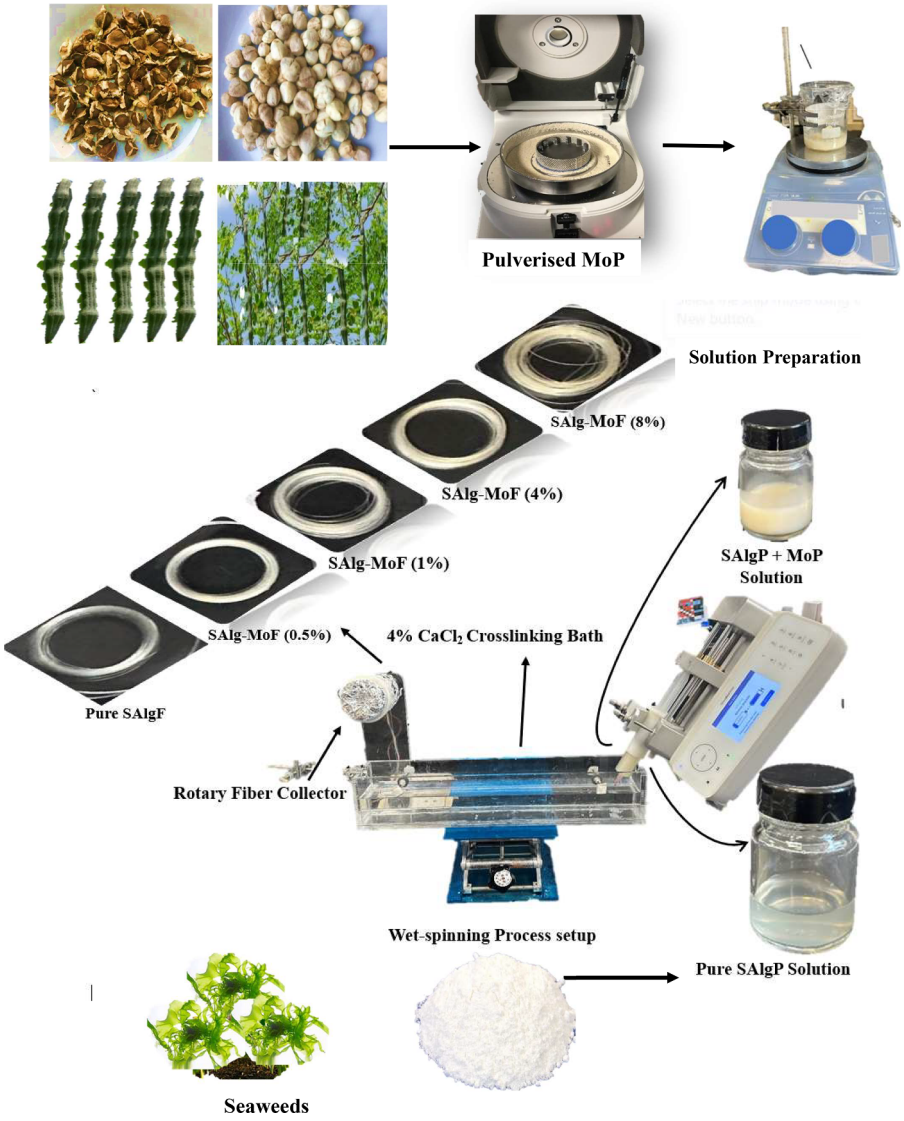


Fig. 1. Synthesis and fabrication process of SAlg-MoF composites through the wet-spinning process, from raw seaweed and seed to final fibre collection.

of pure MoP, pure SalgF, and SAlg-MoF at different concentrations of (0.5 %, 1 %, 4 %, and 8 %).

2.2.5. Selective adsorption experiments

To maintain weight standardisation, 5 mg of each sample of MoP, SAlgF, and composite wet spun fibre SAlg-MoF at different concentrations of 0.5 %, 1 %, 4 %, and 8 % immersed in 5 ml of the solution containing 50mg/L solution containing the heavy metal solution of the Cu^{2+}, Cd^{2+}, and Ni^{2+} aqueous solution of acetates salts. The samples were placed in an orbital shaker set at 200 rpm with a consistent room temperature of 20–25 °C for 24 hours. After this the samples were recovered from the aqueous solution air-dried and later placed in petri dishes and preserved in the desiccation for further analysis.

2.3. Characterisations and instrumentations

2.3.1. Fourier transform infrared (FTIR)

To study the chemical interactions between the FTIR characterisation was conducted on MoP, SAlgP, and SAlg-MoF at different concentrations (0.5 %, 1 %, 4 %, and 8 %), using Nicolet iS™ 10 FTIR Spectrometer from Thermo Scientific™ (Verona, Madison, USA). Measurements were taken with 50 scans at a resolution of 4 cm^{-1} at room temperature, utilising the attenuated total reflectance (ATR) technique with a Smart iTR accessory fitted with a diamond crystal. The recommended Omnic™ software was used for the initial analysis, and Microsoft Excel was used to process the data. The spectral range for the analysis spanned from 4000 to 500 cm^{-1}

2.3.2. Thermogravimetric analysis (TGA) of MoP, SAlgP, SAlgF, and SAlg-MoF

The TGA of the samples was analysed using the available TGA Q500 Thermogravimetric Analyser from TA Instrument, (USA). A conventional TGA was used to determine the weight loss (mg), weight percent loss (wt. %), and rate of weight change in the materials as a function of temperature or time was conducted on samples of pure MoP, SAlgP, SAlgF, and SAlg-MoF (different concentrations). Before the experiment, samples were dried for 2 h in the vacuum oven at a temperature of 40 °C to reduce the moisture contents. Approximately 5 mg of the samples were loaded into the TGA machine using the platinum pan placed in an appropriate pan number. The experiment was conducted using the procedural mode of 1000 °C and a ramp procedural test was conducted. The samples were heated from room temperature heating to the final temperature of 800 °C at a 10 °C/min constant heating rate, under a mass flow control using an inert gas (nitrogen) balanced purge flow of 40 ml/min and a sample purge flow of about 60 ml/min for each experiment.

2.3.3. X-ray diffraction (XRD) MoP, SAlgF, and SAlg-MoF

XRD was conducted on samples of MoP, SAlgF, and SAlg-MoF composite at different concentrations of the fibres. The XRD machine is a Siemens D5005 Rigaku Dual Beam Synergy-S single-crystal X-ray diffractometer (SXRD), Powder X-ray Diffractometer (PXRD) with the operating under radiation condition of Cu Kα radiation (λ=1.54056 Å), operating at 40 kV and 40 mA, range 2θ of 10–90° but 10–55° was computed due to the peaks range. Step width of 0.015° and a counting time of 100 s at each 0.5. The recommended equipment software is DIFFRAC EVA, the software was used to run and obtain the initial analysis result of the X-ray diffraction data before using Origin 2024 and Microsoft Excel software for the analysis.

2.3.4. Scanning electron microscope (SEM) of MoP, SAlgF, and SAlg-MoF

The samples were previously prepared by mounting the individual fibres on the holder and samples used for cross-section observation were fractured with liquid Nitrogen. Before the SEM observation coating was done with a high-purity AU10 (gold) of approximately 10 nm thick, using the Quorum Q150T ES from Quorum Technologies Ltd., Laughton, East Sussex, England, UK. The morphologies of the pure MoP, SAlgF, and SAlg-MoF (different concentrations of 0.5 %, 1 %,4 %, and 8 %) were observed using the Scanning Electron Microscope (SEM), VEGA 4 model, (TESCAN-UK).

2.3.5. Mechanical properties of pure SAlgF and SAlg-MoF fibres

Tensile testing was conducted on samples of SAlgF and SAlg-MoF fibres following the ASTM D3822 - standard test method for tensile properties of single filament fibres, a uniform length of about 8 cm of each sample was prepared, and the fibre samples were affixed onto specialised support tabs designed to mitigate potential distortions or damages arising from the clamping forces during analysis. The test was conducted on each sample fibre using a Mechanical Micro Testing System consisting of Optical Leica using a Leica S9D micro test tensile stage controller Microsystems CH-9435 Heerbrugg (Switzerland) Ltd Singapore, Deben Microtest Tensile Stage Controller using the Deben micro-test software V6.3.4 at 25 °C in a load cell of 5 N under a constant speed rate of 1 mm/min, with a uniform gauge length of about 10.2 mm connected to MT200 single Leadscrew Tensile Tester Digital Extensometer Calibration (Edmunds, Suffolk, UK). A minimum of three independent fibre measurements were done at different sections of the fibre by previous studies (He et al., 2012; He et al., 2020; Hu et al., 2016; Weatherbee-Martin et al., 2016; Yao et al., 2022).

2.3.6. SEM- energy dispersive X-ray spectroscopy (EDX) of MoP, SAlgF, and SAlg-MoF

The Energy-dispersive X-ray Spectroscopy (EDX) Spectral was also recorded on an S8000 model, (TESCAN-UK) UK. Before analysis samples were also coated with high-purity AU10 nm (gold) approximately 10 nm thick, using the Quorum Q150T ES from Quorum Technologies Ltd., Laughton, East Sussex, England, UK. The SEM S8000 was equipped with an ULTIM MAX 100 energy-dispersive X-ray spectroscopy (EDX) system by Oxford Instruments, UK. The EDX of individual samples was conducted simultaneously with the SEM to determine the ffibres' elemental composition and quantify the adsorption of heavy metals (Cu^{2+}, Cd^{2+}, and Ni^{2+}). The accelerating voltage on the SEM is 20ke, on 1nA beam current, Imaging on the secondary electron detector. The Energy-dispersive X-ray Spectroscopy (EDX), Analysis Area: The samples were homogenous during fibre formation and adsorption studies spot analysis mode was used, focusing on selected points of interest on the fibres that showed signs of heavy metal interaction, Spectral Processing: Spectra were acquired with a frame live time of 28 s to ensure comprehensive peak development. which includes automated peak identification and quantification, EDX mapping was done using a processing time of 5 on the resolution of 1024 pixels using the Aztec version 6 software was employed for spectral analysis,

3. Results and discussion

3.1. Fourier transform infrared (FTIR) analysis of the fibres functionalised with mop

Fig. 2 shows the FTIR spectra of the Pure MoP, SAlgP, and the composites fibres SAlg-MoF with various concentrations of 0.5 %, 1 %,4 %, and 8 %, respectively. The profile shows that the existence of the functional groups of MoP and SAlgP is common to the previously reported literature (K. Mishra and Sinha, 2023; Militao, Roddick, Bergamasco, and Fan, 2022)). Such similarity can result in complex behavior of the material as some new peaks and shifts appear in the functionalised samples.

Interestingly, the MoP and SAlgP used were the ones used in our previous studies (Orisawayi et al., 2024), which is evidence of why the results are similar. The broadened cantered peak at 33 12cm^{-1} could be attributed to O–H stretching in main proteins, carbohydrates, fatty acids, and the lignin content structure units and connect to the N–H stretching of amide groups as reported (Dehnad et al., 2024; Elo et al.,

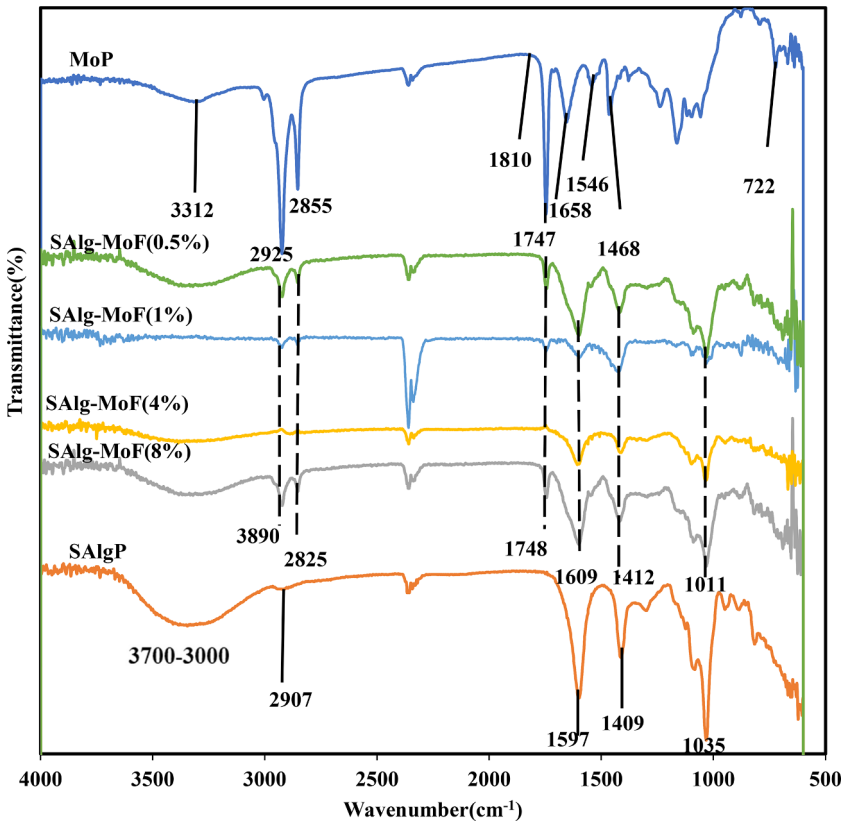


Fig. 2. FTIR spectra comparing the transmittance of MoP, SAlgP, and SAlg-MoF (0.5 %−8 %), composites at varying concentrations.

2024; Sideek et al., 2024). Peaks 2925 and 2855 cm^{-1} respectively are connected to asymmetric and symmetric stretching of–CH in the CH_2 group attributes. The Peaks in 1747 and 1658 cm^{-1} can be attributed to C=O stretching connected to the carbonyl group present in the fatty acid and protein structures, the 1546 cm^{-1} peaks could be related to the main amide group in the protein content of the MoP. The Attributes of C–N stretching and N–H deformation are connected to the peak 1468 cm^{-1}. The unique peak at 722 and 500 cm−1 peaks represents C–H, C–H, CC, and N–H in MoP due to the high percentage of its protein content reported by Araújo et al.

The similar broad peaks in the functionalised samples SAlg-MoF at different concentrations appear broadened as observed in the SAlgP at 3700–3000 cm^{-1} range in all the functionalised samples, this could be due to overlapping of O-H and N-H stretching vibrations, indicating hydrogen bonding within the material (Cai et al., 2023).

The appearance and variations of new peaks specifically 2825 cm^{-1}, 1748 cm^{-1}, 1609 cm^{-1}, 1412 cm^{-1}, and 1011 cm^{-1} in the functionalised samples compared to the pure samples, could suggest new chemical bonds or interactions resulting from the composite complex formation process. Our study agrees with similar studies on alginate functionalisation with different fillers (Gomes et al., 2022); (K. Mishra & Sinha, 2023). Alginate is known as a natural for its excellent gel-forming capabilities (Ramdhan, Ching, Prakash, & Bhandari, 2020). and an abundance of carboxylic groups (Qin, Jiang, & Wang, 2018; Sahoo & Biswal, 2021), the MoP is also known, which contains proteins (Gopalakrishnan, Doriya, & Kumar, 2016) as evidenced by FTIR analysis, The composite SAlg-MoF. could possess the ability to remove impurities including heavy metals, from water. The new composite will be better than when pure MoP or SalgF are used for toxic metal absorption from water to better heavy metal adsorption. The variations and improvement in the mechanical properties when the MoP was added as observed from the result and evidenced by morphology from SEM, is an indication of the incorporation or encapsulation of MoP into the alginate fibre matrix, reinforcing the composite material.

3.2. *Result of the thermogravimetric analysis (TGA-DTG) characterisation MoP, SAlgP, SAlgF, and SAlg-MoF composites*

Fig. 3a, b presents the thermal profile of the combined TGA-DTG Curve of MoP, SAlgP, SAlgF, and SAlg-MoF curve of the composite with different concentrations. while Table 1 presents the details of the relevant thermal degradation temperatures for various samples. Thermo-gravimetric analysis (TGA) of MoP, SAlgP, SAlgF, and SAlg-MoF composite fibres with specific concentrations of 0.5 %, 1 %, 4 %, and 8 %. show distinctive properties that align with previous studies (Apoorva et al., 2020; Kebede, Dube, & Express, 2018; Mehwish et al., 2021; Orisawayi et al., 2024; Savitha, Surendhiran, Balu, & Karthik, 2024; Verdi et al., 2021). The Profile is presented in (Fig. 3a) Pure SAlgP consistently presents step-degradation properties in a range (Darwesh, Mohamed, and Soliman, 2024; Dodero, Alloisio, Vicini, & Castellano, 2020; Jadbabaei, Kolahdoozan, Naeimi, & Ebadi-Dehaghani, 2021; Sattariazar, Nejad Ebrahimi, & Arsalani, 2023) It was observed that the first stage occurs at 40 °C and extends to a temperature range of about 110 °C, with a weight loss of 1.2 mg, about 10 % wt over the temperature range. This stage is Ascribed to the evaporation of entrapped water, volatile compounds, or moisture within the SalgP (Orisawayi et al., 2024; Safaei & Moghadam, 2022). In the second stage, the thermal degradation starts at temperatures between 225 and 270 °C, with weight loss increasing to 3.5 mg at approximately 32 % wt; this can be ascribed to the final release of structural water in the SAlgP. The third stage occurs between approximately 310 and 515 °C with a weight stabilisation at about 1 mg at 10 %wt. this can be ascribed to the thermal stability of alginate's polysaccharide. (Vincent et al., 2020). The final stage could be attributed to the decomposition stage of the SAlgP, this occurs at temperatures above 570 °C the weight loss beyond this stage measured to 789 °C presents a weight loss of 1.3 mg at approximately 12 % wt. This

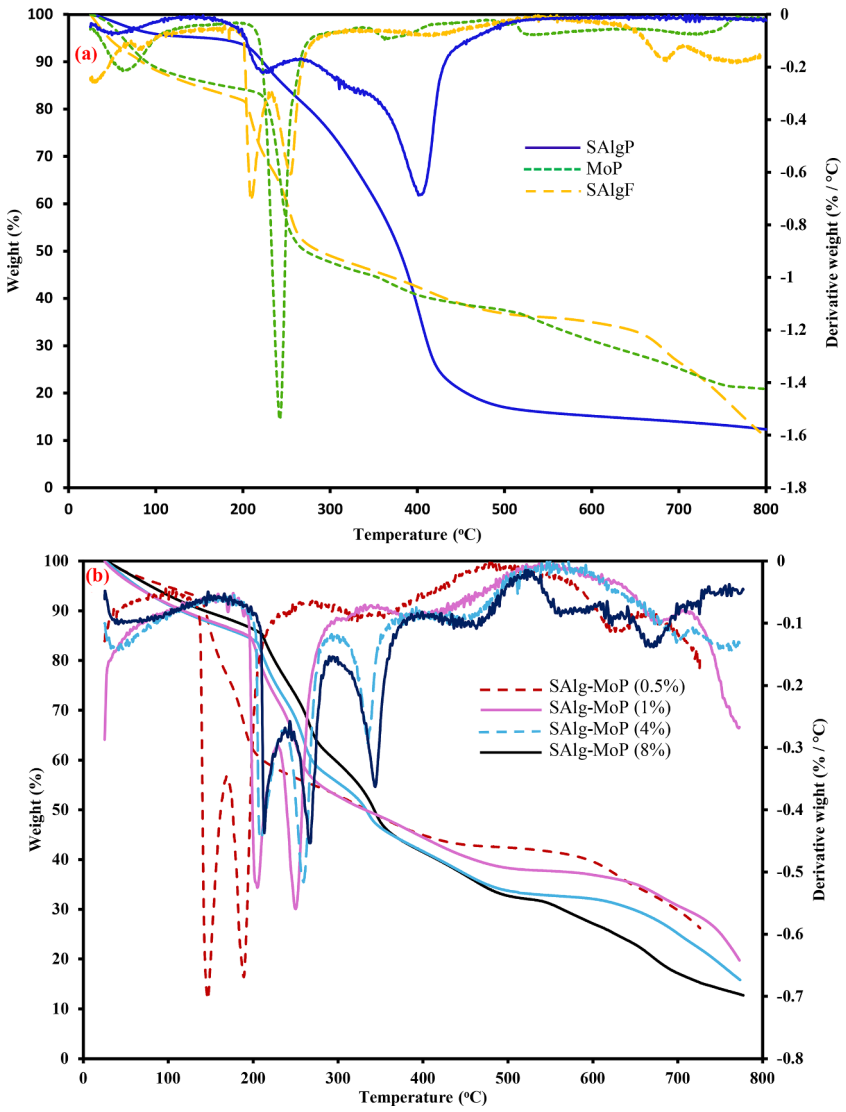


Fig. 3. (a) Combine TGA-DTG Curve of MoP, SAlgP, and SAlgF; (b) Combine TGA-DTG of the SAlg-MoF curve of the composite with different concentrations.

Table 1
Thermal degradation temperatures for various samples.

Sample	$T_{5\%}$ (°C)	$T_{10\%}$ (°C)	$T_{50\%}$ (°C)	$T_{peak\ 1}$ (°C)	$T_{peak\ 2}$ (°C)	$T_{peak\ 3}$ (°C)
MoP	159.07	222.54	379.66	401.55	–	–
SAlgP	62.37	89.30	271.80	241.50	–	–
SAlgF	46.13	83.60	287.51	209.55	254.50	–
SAlg-MoF (0.5 %)	96.76	143.65	333.45	147.55	189.48	–
SAlg-MoF (1 %)	63.82	118.42	326.45	206.55	251.65	–
SAlg-MoF (4 %)	62.89	114.66	326.45	210.02	258.01	334.02
SAlg-MoF (8 %)	78.66	142.63	342.24	213.04	267.30	344.32

phase is due to the breakdown of the metal-carbon present in the SAlgP. Findings agree with previous studies (Ananth et al., 2024; Bargavi, Balakumar, & Raghunandhakumar, 2024; Orisawayi et al., 2024; Varughese, Gokul, & Keerthi, 2024). The thermal behaviours of the MoP, when compared with degradation patterns observed in the previous literature, show three major thermal degradation processes (Balogun et al., 2021; Fu et al., 2021; Yadav, Rhee, & Park, 2014). The first stage is primarily a result of the evaporation of water and the probable loss of volatile, low molecular weight compounds entrapped within the MoP with the onset temperature starting from 33 to 133 °C with a loss of weight of 0.32 mg at 4 % wt. The Second event shows and is an attribute of degradation of the amine group and amino acids reported to be present in the high protein contents of MoP, at this stage, some other gaseous products, like carbon dioxide (CO2) and some traces of ammonia (NH_3) gases, may be given off during the form during the degradation process (Verdi et al., 2021). This weight loss phase event occurs at 210 to temperatures of approximately 325 °C 1.8 mg 24 % wt. The third degradation stage occurs at 349 °C and approximately 430 °C resulting in a 2.8 mg at about 37 %wt. This corresponds to complete pyrolysis of most organic components, such as fatty acids, antioxidants, vitamins, and other dietary fibres, including lignin, and cellulose present in seed biomass capable of undergoing significant thermal degradation, contributing to the formation of the final char (Araújo, Melo, Alves, & Coelho, 2010; Bhutada et al., 2016; Gharsallah et al., 2023; Magalhães Souza et al., 2022; Santos, de Jesus, da Silva, and Pontes, 2020). The wet-spun SAlgF crosslinked with 4 % $CaCl_2$ presents enhanced thermal stability, with a degradation onset at 206.61 °C and significant weight loss between 209 °C to 260 °C at approximately 24.102 % wt. This enhancement could be attributed to the increased thermal resistance of the polymer packing efficiency and intermolecular interactions in the SAlgP molecules during the crosslinking process in the wet spinning

process coagulation bath. The enhancement is advantageous and could be extremely useful to explore composites with applications that involve exposure that requires high temperatures with robust thermal resistance stress (Hufenus, Yan, Dauner, & Kikutani, 2020; Marsano et al., 2005; Tang et al., 2018). SAlg-MoF composite fibres with specific incorporation of MoP concentrations with 0.5 %, 1 %, 4 %, and 8 %. This modification significantly influenced the thermal degradation of SAlgF. The composites showed progressive changes in thermal degradation patterns, with alterations in the onset temperatures and weight loss percentages, reflecting the impact of more MoP concentration on the thermal stability of the alginate matrix. Specifically, SAlg-MoF (0.5 %) indicates the interaction between the MoP concentration effect on the pure SAlgP matrix by exhibiting an onset of degradation at 207.71 °C, this could be a reinforcing effect of the addition of 0.5 % of MoP into the composites, therefore affecting the thermal stability as compared with the SAlgF. The SEM results also confirm the material's structure was altered at different concentrations. SAlg-MoF (1 %) could create a link within the SAlg matrix by effectively distributing thermal energy that could hinder the movement of the degradation of the composites resulting in a delay in the onset of degradation and final degradation it also has the highest mechanical strength from the mechanical with also a significant improvement in thermal stability from the TGA experiment. The SAlg-MoF (4 %) and SAlg-MoF (8 %) show a is progressive change in degradation patterns with higher concentrations, implying that more increase in the addition of MoP with effects on the SAlgF.

Results from the DTG curves of pure MoP and SAlgP, also shown in Fig. 3a, exhibit distinct transition phase peaks cantered at 401.55 °C and 241.50 °C, respectively, these peaks are similar 8to the primary degradation stages previously reported in the literature (Coldebella et al., 2024; Freitas, Vidart, da Silva, & Vieira, 2021; Popa, Lisa, & Aelenei, 2008).

The thermal decomposition of SAlgF, characterised by a major peak at 209.55 °C and a secondary peak at 254.50 °C, could be attributed to the crosslinking effect of $CaCl_2$ on the SAlgP solution, enhancing its thermal stability. In contrast, the SAlg-MoF composites (Fig. 3b) exhibit more complex degradation behavior. The SAlg-MoF(0.5 %) and SAlg-MoF (1 %) samples display two distinct degradation peaks, with the decomposition temperatures increasing as the Moringa content rises. Specifically, SAlg-MoF (0.5 %) shows peaks at 147.55 °C and 189.48 °C, while SAlg-MoF(1 %) exhibits peaks at 206.55 °C and 251.65 °C. For the higher MoP loadings of SAlg-MoF (4 %) and SAlg-MoF (8 %), multiple degradation stages were observed. For higher MoP- loadings, such as in SAlg-MoF(4 %) and SAlg-MoF (8 %), multiple degradation stages were observed. SAlg-MoF (4 %) exhibited peaks at 210.02 °C, 258.01 °C, and 334.02 °C, while SAlg-MoF(8 %) displayed peaks at 213.04 °C, 267.30 °C, and 344.32 °C, reflecting more complex thermal degradation behavior. The broader and more peaks suggest enhanced interactions between the SAlg matrix and MoP, contributing to the increased complexity of the degradation process. These results suggest that the MoP significantly alters the thermal stability and degradation of the composites.

3.3. X-ray diffraction (XRD)

Fig. 4 shows the series of diffractograms of each analysed sample of the MoP, SAlgF, and SAlg-MoF at different concentrations of 0.5 %, 1 %, 4 %, and 8 %, respectively. Previously reported studies have shown that the XRD pattern of the Mop demonstrated poorly resolved peaks (Abatal et al., 2021). As an indication of the predominant nature of the biosorbent containing abundant protein compounds which could facilitate the absorption of heavy metal more easily on the surface (Chowdhury & Saha, 2011; Madala et al., 2017). The resolved peak of the MoP is similar peaks with few variations with typical peaks obtained from *M. Oleifera* seed and leaves powder due to the similarity in their constituents (Kouadio et al., 2024; Masitlha, Seifu, & Teketay, 2024; Ortolá et al., 2024; Susanto et al., 2023). Notable peaks were observed at 2θ values of approximately17.0°, 20.09 °, 23.3 °, 26.3 °, 38.36 °, and 42.1 °, 44.7 °, and 59.1 °, exhibiting minor variations and shifts compared to previous studies, potentially due to the complex matrix of proteins, vitamins, lipids, and lignin nature present in the MoP, these results align with similar findings reported (Elkhatib, Mahdy, & Salama, 2015; Hamadeen, Elkhatib, Badawy, & Abdelgaleil, 2021; Susanto et al., 2023). SAlgF demonstrated a sharp crystallographic peak 2θ at 13.7, 26.02 °, and 40.4 different from that of the MoP and the composites with similar peaks like that of crosslinked sodium alginate's crystalline structure pattern with different peaks (Gover Antoniraj, Maria Leena, Moses, & Anandharamakrishnan, 2020; Hua et al., 2010; Kalyani, Smitha, Sridhar, & Krishnaiah, 2006; Kolanthai et al., 2018); (Z.-H. Zhang et al., 2022). The composite SAlg-MoF at a 0.5 % concentration showed peak patterns like other composites, with new peaks at 17.2 different from those obtained

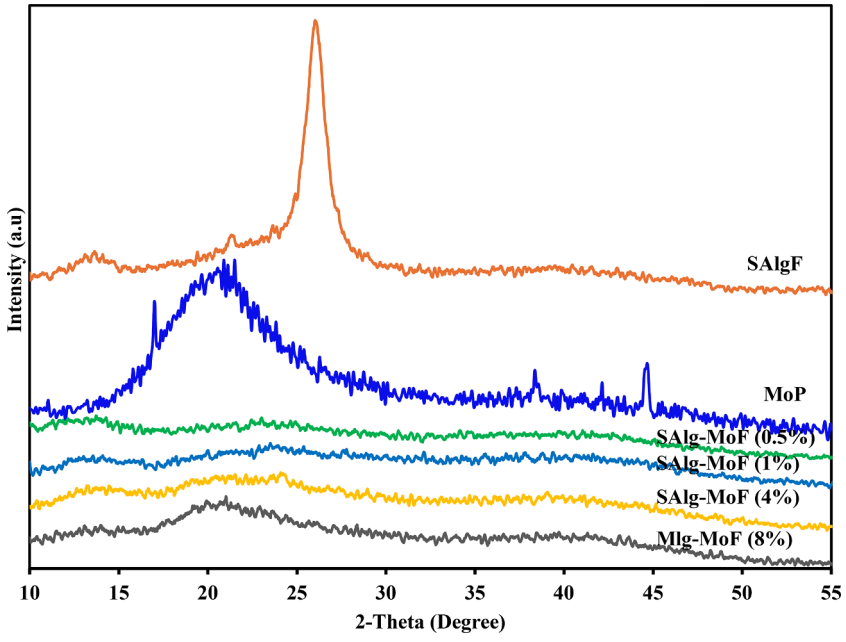


Fig. 4. X-ray diffraction (XRD) patterns analysis of MoP, SAlgF, and SAlg-MoF composites (0.5 %, 1 %, 4 %, and 8 % MoP) indicating phase composition.

from SAlgF. These peaks shifted to 20.2 ^{o} and 19.1 ^{o} at concentrations of 1 %, 4 %, and 8 %, respectively, this reflection could be because of an increase in the incorporation of Mop into the composites. This incorporation confirms the structural integration of Mop at higher concentrations as observed and confirmed by the SEM analysis, which may have caused the composite morphology to change as also evidenced by the mechanical and thermal change in different degradation properties.

3.4. SEM structure morphology of MoP, SAlgF, and SAlg-MoF composite fibres

Fig. 5 shows the morphology of the images observed from scanning electron microscope (SEM) characterisations at an appropriate magnification of the individual MoP, SAlgF, and SAlg-MoF of different concentrations from the traditional wet-spinning process.

3.4.1. Observation from the MoP particles

The SEM images in (Fig. 5a_1, a_2) reveal the morphology of MoP particles exhibiting both uniform and spherical sizes and shapes. This characteristic is typically associated with naturally pulverised materials as compared with previous studies (Huang et al., 2020). The use of a high magnification from the SEM images provides more details on the Structure. The observed morphology possessed a heterogeneous and porous matrix like that of the *Moringa* stenopetala seed powder from a study conducted by Temesgen et al. (Kebede et al., 2018). A similar nature to the morphology study is also in agreement with the study on the investigation of grounded *M. Oleifera* seed used for the application of the interface of food and medicine (Gharsallah et al., 2023; Verdi et al., 2021). In the current study dimensions measured across different particles indicate different broad distributions with a mean size of approximately 6.94 μm (±1.52) with an average area of about 39.64 μm^2 assuming the particles are spherical. The nature of the MoP could be attributed to the mechanical force induced on the seed during the

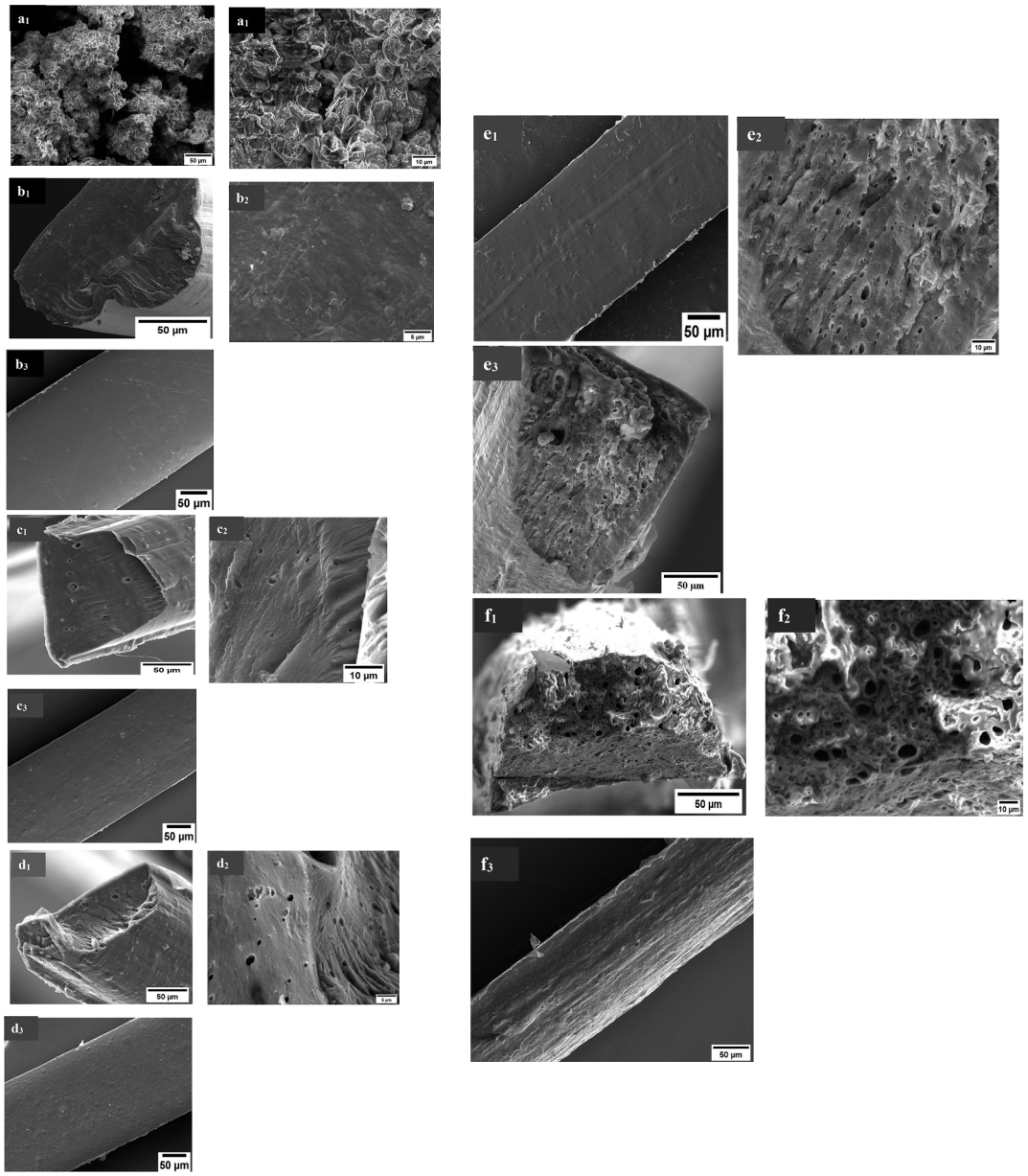


Fig. 5. Scanning electron microscopy (SEM) images displaying morphological details of materials at different magnifications. MoP (a_1: 800x, a_2: 3000x), SAlgF cross-sections (b_1: 800x, b_2: 3000x) and surface (b_3: 800x), along with SAlg-MoF composites (0.5 %−8 % MoP; c_1-f_3) at 800x and 3000x magnifications to show morphological variations.

pulverisation process reported by studies on grinding by (Huang et al., (2020); Huang et al., (2020); Zhao, Zhu, Chen, & Ao, (2015)) more. The detailed structure shows particle structure also possesses materials with lots of structural interlocking. Considering its properties, MoP could offer a cost-effective and promising method of addressing impurities absorption. As a result of its attribute to its protein content as confirmed by the FTIR analysis. There could be a potential for adsorption capacity in water treatment applications, as reported that similar structures can facilitate the morphology profiles that can be used for water treatment specifically the heavy metals (Araújo et al., 2010; Gopalakrishnan, Doriya, & Kumar, 2016; Kebede et al., 2018). In addition, this profile has contributed to the improved mechanical and thermal stability properties when used as a filler in various applications, including water treatment as by the mechanical properties of the fibre developed from the wet spun fibre.

3.4.2. Sodium alginate fibres (SAlgF)

Fig. 5 b_1, b_2, and b_3 show the morphology of the cross-section at different magnifications, and the surface of pure SAlgF is shown in and when observed exhibits the characteristic nature of a smooth homogenous surface with consistent fibre diameter. There was no core shell or collapsed structures on the surface and the cross-section of the fibre was expected from an unmodified pure SAlgF. The morphology is like studies observed in the literature (Li et al., 2024); (T. Wang et al., 2024) and other literature from pure wet spinning processes based on many cellulose nanofibrils (Z. Zhang et al., 2024). However, there are no signs of surface particulates or porous materials, these fibres were straight, with noticeable streak patterns observed on their surfaces. indicating a tightly packed polymeric structure with similar studies from literature on pure SAlgF and some polymeric wet-spun fibre (Wade et al., 2017; Watthanaphanit et al., 2010). This fibre is a good result for comparing the impact of MoP when incorporated.

3.4.3. Effects of MoP incorporation on fibre morphology

The incorporation of 0.5 % Mop observed in (Fig. 5c1, c_2, and c_3) reveals lightly noticeable changes on the surface, with a barely obvious layer. Further increment in MoP particles of fibre-product SAlg-MoF (1 %) (Fig. 5 d_1, d_2, and d_3) with the incorporation of MoP at 1 % shows a noticeable pronounced roughness with a slightly porous structured suspension during the solution preparation and the wet spinning process. The SAlg-MoF (4 %) in (Fig. 5 e_1, e_2, and e_3 as the wet-spun composites increase, the surface roughness and some little pore formation. This could be an indication of a massively loaded MoP causing alteration of the fibre surface and cross-sectional and the internal morphology and reduction in the mechanical properties. The fibre SAlg-MoF (8 %) shown in (Fig. 5 f_1, f_2, and f_3) composites revealed the most dramatic observable morphological structural changes with a highly irregular and porous surface structure. This morphology can be seen as inhomogeneous when observed across the sections in the section and the surface. This could have been a result of the reflecting massive MoP within the fibre structure, providing weak mechanical properties. The behavior connects to several wet-spun fibres related to alginate from several studies (J. Wang et al., 2010; Li et al., 2024; Lin, Wang, Wertheim, & Coombes, 2017; Park et al., 2021; Sibaja et al., 2015; Ureña-Benavides, Brown, & Kitchens, 2010)

Implications for different applications including water treatment is that the morphological characteristics at each MoP concentration at different levels suggest different effects and alterations in the capacity, thermal stability, shifts in peaks of the Xray-diffraction and mechanical properties of the SAlg-MoF fibres. However, we expect the observed pore distribution and increase in the surface roughness across the functionalised fibres could be expected to correlate positively with an enhanced capture of contaminants.

3.5. Mechanical characterisation of the pure SAlgF and SAlg-MoF composites

The mechanical characterisation of the SAlgF and SAlg-MoF composites with the MoP concentrations (0.5 %, 1 %, 4 %, and 8 %) was investigated to determine how each concentration influences the mechanical properties of the composites. The results from the stress-strain curves from the SAlgF and SAlg-MoF composites under tensile loading are shown in (Fig. 6). The ultimate tensile strength (UTS), breaking strain, and Young's modulus (YM) results from the experiment are presented in (Fig. 7). While that of the Young's modulus (YM) are presented in (Fig. 8). It was observed for both the UTS and YM exhibited a consistent trend, indicating reliable mechanical behavior across the tested samples.

The initial UTS value obtained from the pure polysaccharide alginate polymer (SAlgF) obtained after cross-linked with 4 % $CaCl_2$ is approximately 10.81 MPa (±1.37), and the YM value is about 0.36 GPa (±0.76). The introduction of 0.5 % MoP increased the UTS to 31.05 MPa (±1.57) and the YM to 1.48 GPa (±0.10), indicating a significant improvement in the mechanical properties of the fibres compared to the pure SAlgF fibres.

Further increment in the MoP of 1 % concentration showed a significantly highest value of UTS of 65.32 MPa (±7.20), with a YM of 2.93 GPa (±0.89). Deduction from these findings should have an approximate value of about 6.04 times greater than the SAlgF cross-linked with 4 %, resulting in a significant enhancement of the composite's mechanical properties. The increase in strength of the composited could be attributed to the interaction compatibility and homogeneity of the carbohydrate polymer matrix SAlgP, and MoP fillers in the composites and the strong interaction between alginate macromolecules and the MoP. Studies have reviewed that. enhancing the properties of carbohydrate alginate-based materials polymers through multiphase formulation through additional design and processing innovation could improve the mechanical properties of the alginate matrix and review based on source modification methods, the potential applications of alginate-based modified polymers (Kumar, Singh, & Kumar, 2024). Similar studies were observed in studies conducted on alginate loaded with fillers (He et al., 2012; Wu et al., 2023). However, the SEM in (Fig. 6), also shows visible features of homogeneous dispersion of MoP particles in the composite's matrix, which could also contribute to the improved mechanical properties of the SAlg-MoF composites.

However, MoP concentrations at MoP at 4 % and 8 % MoP, show a distinct decline in the mechanical properties. Reducing UTS value to 45.19 MPa (±4.91) and 26.51 MPa (±4.34) for the 4 % and 8 % MoP composites respectively, while the YM decreased to 2.05 GPa (±1.37) at 4 % MoP and finally to 1.66 GPa (±0.35) at 8 % MoP.

Conclusively, the SAlg-MoF at MoP (1 %) exhibits the highest breaking strain point compared to the other composites. There was a progressive decrease from 24.07 % in pure SAlgF to 7.51 % in the composite with an 8 % MoP concentration. This decrease could be attributed to a weakness in the interface bonding which may be caused by agglomeration of polysaccharide matrix on further addition MoP particles, which could lead to easier crack propagation within the structures of the composites (Sampath & Santhanam, 2019; Vázquez-Guerrero et al., 2021). The mechanical and structural properties indicate that there can be a wide range of mechanical properties within the new SAlg-MoF composite assembly. These findings are similar and in agreement with some previous studies (Akbari et al., 2014; Al-Hasani, Hamad, and Faheed, 2024)

3.6. SEM- energy dispersive X-ray spectroscopy (EDX) MoP, SAlgF, and SAlg-MoF

The SEM-EDX analysis was performed on the adsorbents MoP, SAlgF, and SAlg-MoF with different concentrations (0.5 %,1 %,4 %, and 8 %) to focus on the relevant elements. We have streamlined the key elements to

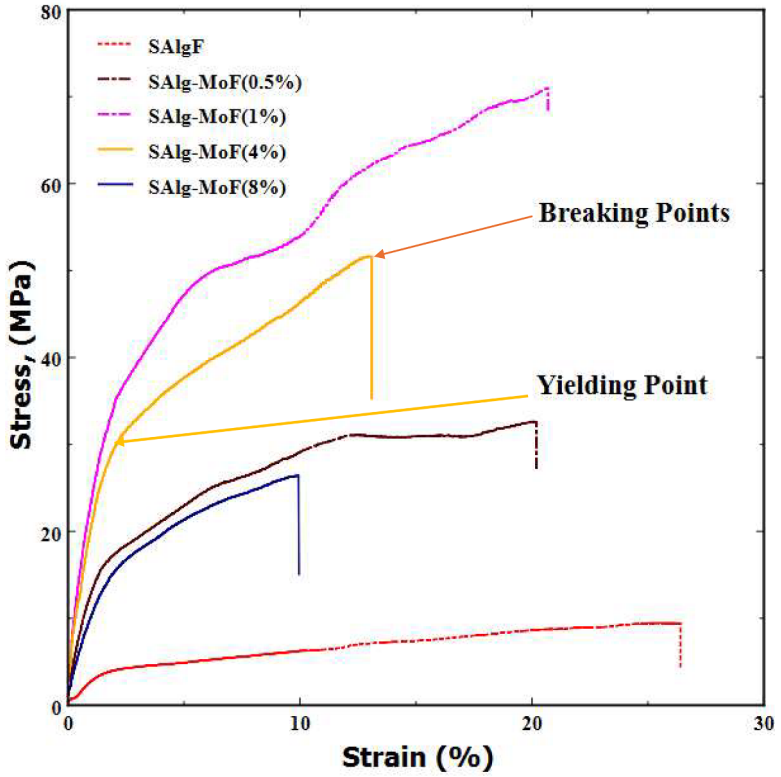


Fig. 6. The stress-strain curves of the SAlgF and SAlg-MoF composites.

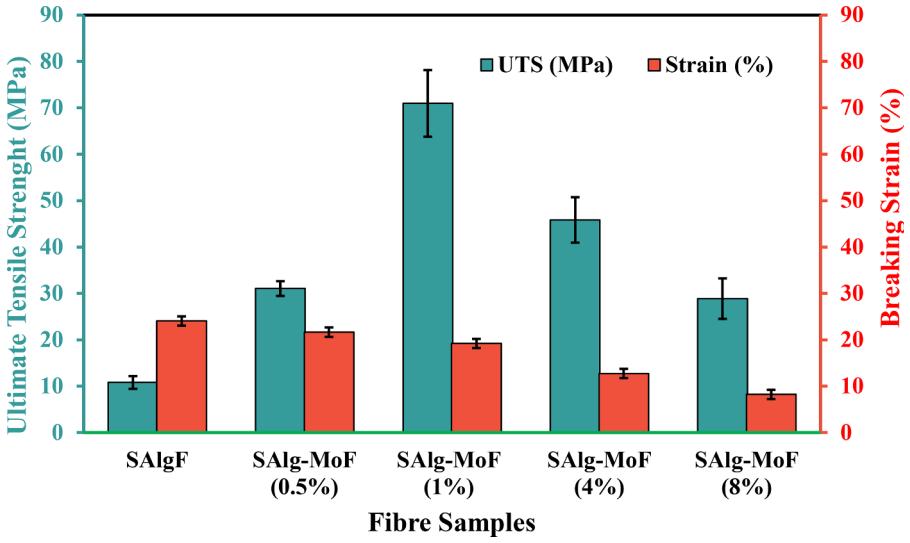


Fig. 7. Combination plot of the ultimate tensile strength and breaking strain of SAlgF and SAlg-MoF Composites.

focus on those applicable to the adsorption studied. During the analysis, The EDX software automatically adjusted the remaining elements' percentages to 100 %, ensuring a clear and focused representation of the significant elements detected.

Fig. 9 illustrate the detailed SEM-EDX morphology and elemental peaks for SAlg-MoF (4 %) composites before adsorption, MoP, SAlgF, and SAlg-MoF at different concentrations after selective adsorption of heavy ions. The result from (Fig. 9a) shows notable peaks of the pristine nature which were attributes related to trace elements such as Manganese (Mg), potassium (K), Phosphorus (P) Sulphure (s), and Calcium (Ca) found in previous elemental analysis from previous studies of MoP and SAlgF (Ravikumar & Mater, 2020)

The detection of cadmium (Cd), copper (Cu), and nickel (Ni) after adsorption confirms the successful capture of these heavy metals by the adsorbents as these were not present in the pure MoP, SAlgF of the SAlg-MoF Composites. Therefore, the comparative features of the morphology features of the materials and composites are uneven and heterogeneous with some pores. A similar observation was also found in literature studies by Ravikumar and Udayakumar (Ravikumar & Mater, 2020). with lots of irregular and uneven surfaces in their composites after it was used for adsorption as some of these pores could facilitate adoption.

Comparing the EDX spectra of SAlgF and SAlg-MoF shows distinct differences in their ability to adsorb heavy metals. SAlg-MoF exhibits

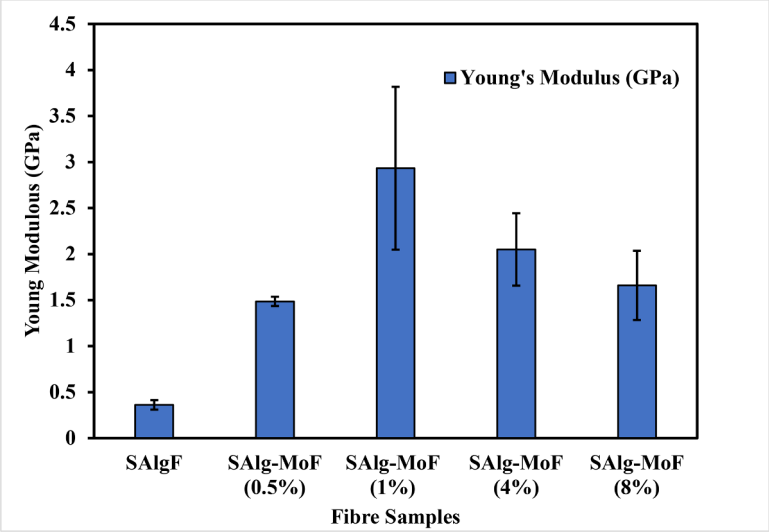


Fig. 8. Typical Young modulus of SAlgF and SAlg-MoF Composites.

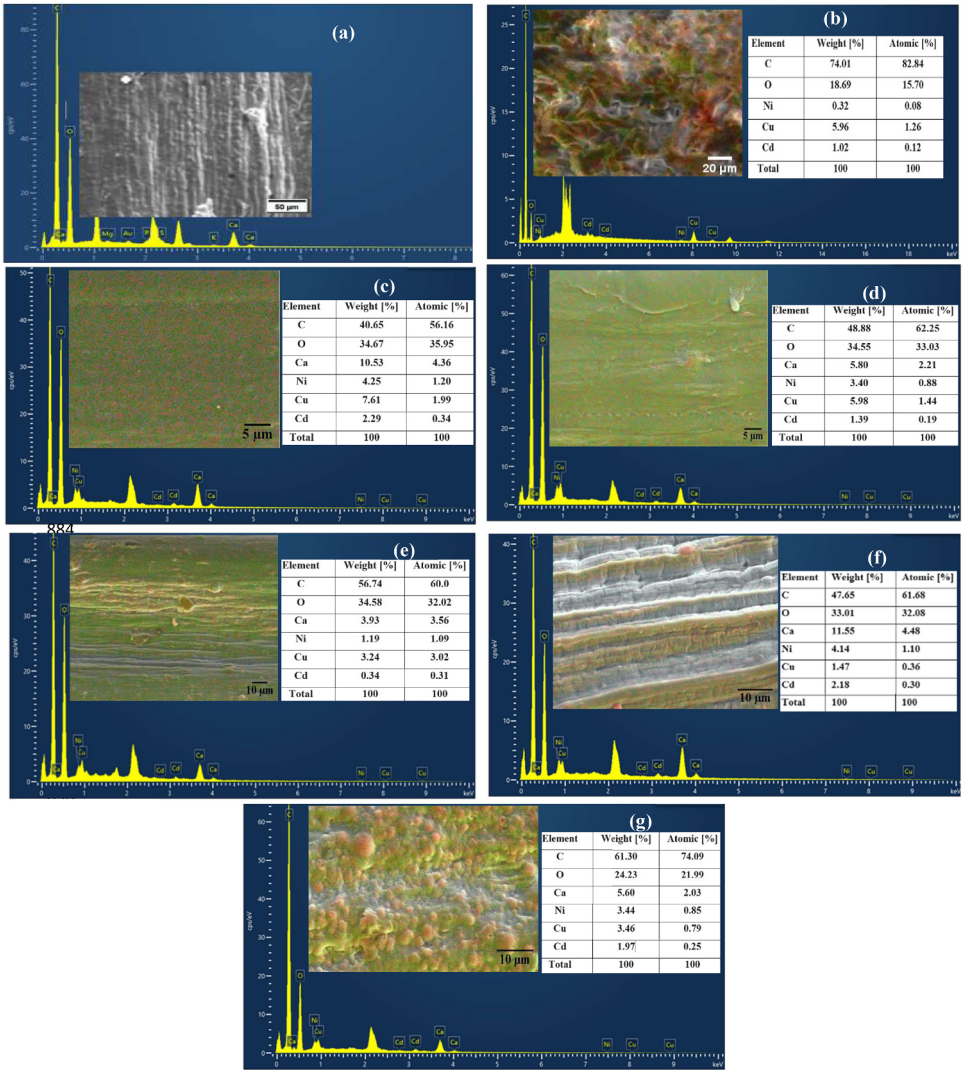


Fig. 9. Detailed SEM-EDX morphology and elemental peaks of composites: (a) Pure SAlg-MoF (0.4 %), (b) Absorbed MoP (b), (c) SAlgF, and SAlg-MoF (d) 0.5 %, (e) 1 %, (f) 4 %, and (g) 8 %, after selective adoption of heavy ions ($Cu^{2+,}$ $Ni^{2+,}$ and Cd^{2+}).

higher peaks for Cu, Ni, and Cd after adsorption, indicating a higher affinity and capacity for these metals compared to SAlgF in Fig. 9.

Fig. 10 presents the SEM-EDX mapping of SAlg-MoF at 1 % MoP concentration, the feature shows that the metal ions are distributed and homogeneously of the heavy metal ions captured within the matrix. The maping shows the spatial distribution within the SAlg-MoF matrix and highlighted theheavy metal ions are evenly distributed throughout the adsorbent material, indicating effective and uniform adsorption. The deduction from the studies shows that the material not only captures heavy metal ions effectively but also distributes them homogeneously within its structure, ensuring consistent performance and this could facilitate a high adsorption capacity. This makes SAlg-MoF promising composites for removing heavy metals from contaminated water.

4. Conclusions

In this study, we successfully developed and characterised sustainable sodium alginate-*M. oleifera* composite fibres (SAlg-MoF) using a green wet-spinning process. The composites were synthesised with varying concentrations of MoP (0.5 %, 1 %, 4 %, and 8 %) and reinforced into SAlgF. The fibres were characterised, and selective adsorption studies were conducted in aqueous solutions containing Cu^{2+}, Cd^{2+}, and Ni^{2+} ions. Our findings confirmed that incorporating MoP into SAlgF significantly improved mechanical and thermal properties while preventing MoP particle leaching after adsorption. Moreover, the preliminary selective adsorption studies demonstrated the effectiveness of the composite fibres in capturing heavy metal ions, with no detectable metal traces on the fibres surface after adsorption, as confirmed by SEM-EDX analysis. These results validate the fibres' feasibility as sustainable, biodegradable materials for water purification. Future research will explore the adsorption and absorption, kinetics and adsorption isotherm in details using established models to assess the long-term stability, reusability, and overall effectiveness of the fibres in removing various contaminants. This study not only confirms the initial hypothesis but also highlights the potential of natural materials in developing advanced bio-composites with multifunctional properties.

Data availability

The data and supporting documents are available upon reasonable request from the corresponding.

CRediT authorship contribution statement

Abimbola Oluwatayo Orisawayi: Writing – review & editing, Writing – original draft, Visualization, Software, Project administration,

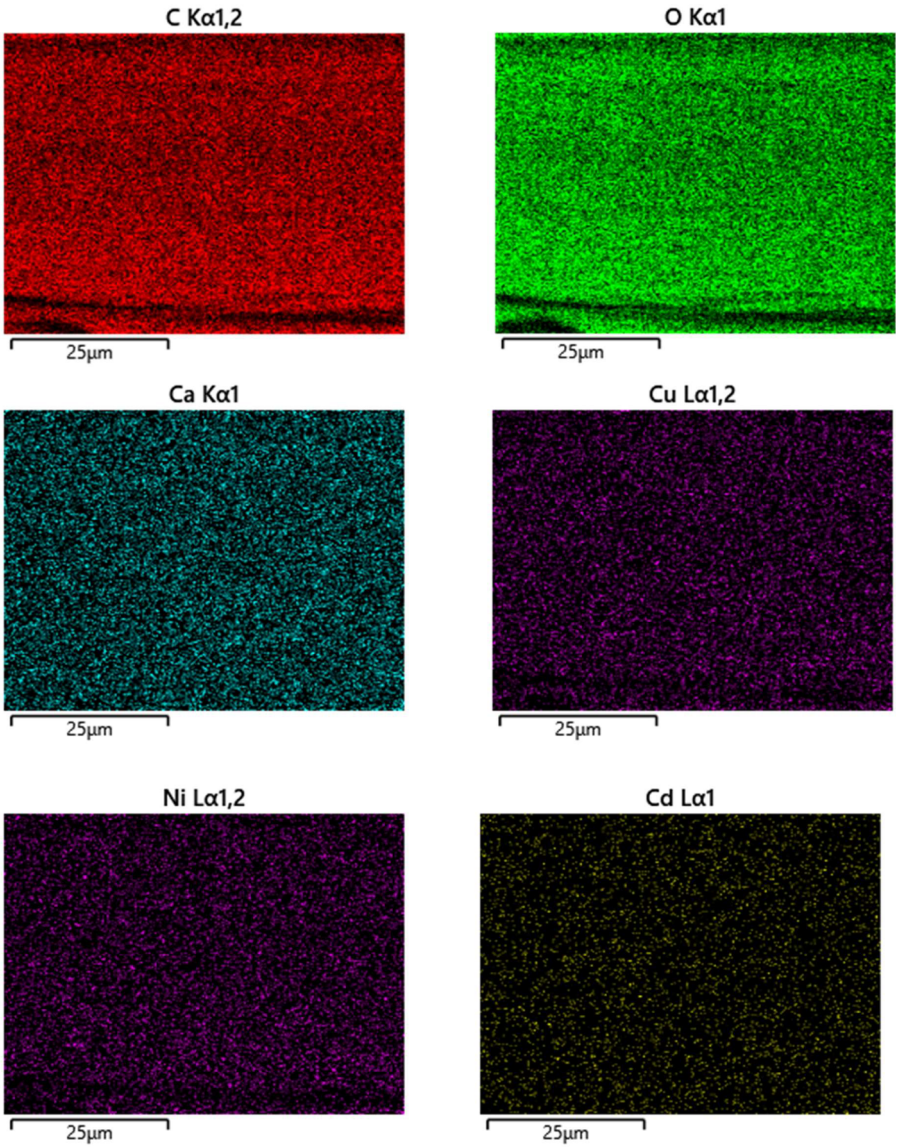


Fig. 10. SEM-EDX mapping of SAlg-MoF (1 %).

Methodology, Investigation, Funding acquisition, Formal analysis, Conceptualization. **Krzysztof K. Koziol:** Writing – review & editing, Visualization, Software, Methodology, Formal analysis, Conceptualization. **Sameer S. Rahatekar:** Writing – review & editing, Visualization, Supervision, Software, Methodology, Formal analysis, Conceptualization.

Declaration of competing interest

The authors declare that they have no known competing financial interests or personal relationships that could have appeared to influence the work reported in this paper.

Acknowledgments

The authors would like to acknowledgment the financial support of Petroleum Technology Development Fund (PTDF) of the Federal republic of Nigeria, through the award of Postgraduate Scholarship at the Ph.D. level, NO. PTDF/ED/OSS/PHD/AOO/1844/2020PHD152. Special acknowledgment is extended to Jim Hurley, Diane Johnson, Kris Bramley, and Christine Kimpton for their assistance with SEM, EDS, and XRD analysis, and to Dr. David Ayre for his training on TGA. Finally, thanks to all the staff of the Composites and Advanced Materials Centre, Faculty of Engineering and Applied Sciences, at Cranfield University for their invaluable technical support and encouragement during the experimental work.

Supplementary materials

Supplementary material associated with this article can be found, in the online version, at doi:10.1016/j.carpta.2024.100620.

Data availability

Data will be made available on request.

References

Abatal, M., Olguin, M., Anastopoulos, I., Giannakoudakis, D., Lima, E., Vargas, J., et al. (2021). Comparison of heavy metals removal from aqueous solution by Moringa oleifera leaves and seeds. *Coatings, 11*(5), 1–14. https://doi.org/10.3390/coatings11050508

Akbari, M., Tamayol, A., Laforte, V., Annabi, N., Najafabadi, A. H., Khademhosseini, A., et al. (2014). Composite living fibers for creating tissue constructs using textile techniques. *Advanced Functional Materials, 24*(26), 4060–4067. https://doi.org/10.1002/adfm.201303655

Al-Hasani, F. J., Hamad, Q. A., & Faheed, N. K. (2024). Enhancing the cell viability and antibacterial properties of alginate-based composite layer by adding active particulates. *Discover Applied Sciences, 6*(2), 1–6. https://doi.org/10.1007/s42452-024-05715-6

Amin, M. F., Ariwibowo, T., Putri, S. A., & Kurnia, D. (2024). Moringa oleifera: A review of the pharmacology, chemical constituents, and application for dental health. *Pharmaceuticals, 17*(1), 100–122. https://doi.org/10.3390/ph17010142

Ananth, K. P., Paul, P. K., Paliwal, H., Nath, V., Nakpheng, T., & Srichana, T. (2024). Controlled degradation and kinetics response in calcium silicate doped with sodium alginate/functionalized multi-walled carbon nanotube composite 3D scaffolds for cartilage regeneration. *Journal of Materials Research and Technology, 29*, 4978–4990. https://doi.org/10.1016/j.jmrt.2024.02.178

Apoorva, A., Rameshbabu, A. P., Dasgupta, S., Dhara, S., & Padmavati, M. (2020). Novel pH-sensitive alginate hydrogel delivery system reinforced with gum tragacanth for intestinal targeting of nutraceuticals. *International Journal of Biological Macromolecules, 147*, 675–687. https://doi.org/10.1016/j.ijbiomac.2020.01.027

Araújo, C. S. T., Alves, V. N., Rezende, H. C., Almeida, I. L. S., de Assunção, R. M. N., Tarley, C. R. T., et al. (2010). Characterization and use of Moringa oleifera seeds as biosorbent for removing metal ions from aqueous effluents. *Water Science and Technology, 62*(9), 2198–2203. https://doi.org/10.2166/wst.2010.419

Araújo, C. S. T., Melo, E. I., Alves, V. N., & Coelho, N. M. M. (2010). Moringa oleifera Lam. seeds as a natural solid adsorbent for removal of AgI in aqueous solutions. *Journal of the Brazilian Chemical Society, 21*(9), 1727–1732. https://doi.org/10.1590/S0103-50532010000900019

Balogun, A. O., Adeleke, A. A., Ikubanni, P. P., Adegoke, S. O., Alayat, A. M., & McDonald, A. G. (2021). Kinetics modeling, thermodynamics and thermal performance assessments of pyrolytic decomposition of Moringa oleifera husk and Delonix regia pod. *Scientific Reports, 11*(1), 1–12. https://doi.org/10.1038/s41598-021-93407-1

Bargavi, P., Balakumar, S., & Raghunandhakumar, S. (2024). Multi-functional bandage - bioactive glass/metal oxides/alginate composites based regenerative membrane facilitating re-epithelialization in diabetic wounds with sustained drug delivery and anti-bactericidal efficacy. *International Journal of Biological Macromolecules, 262*, 1–22. https://doi.org/10.1016/j.ijbiomac.2024.130054

Behrooznia, Z., & Nourmohammadi, J. (2024). Polysaccharide-based materials as an eco-friendly alternative in biomedical, environmental, and food packaging. *Giant, 19*, 1–20. https://doi.org/10.1016/j.giant.2024.100301

Benettayeb, A., Masamvu, J. M., Chitepo, R. M., Haddou, B., Sillanpaa, M., & Ghosh, S. (2024). Facile fabrication of new bioadsorbents from Moringa oleifera and alginate for efficient removal of uranium(VI). *Journal of Radioanalytical and Nuclear Chemistry, 333*(5), 2369–2387. https://doi.org/10.1007/s10967-024-09470-1

Bhatia, S., Othman, Z., & Ahmad, A. L. (2006). Palm oil mill effluent pretreatment using *Moringa oleifera* seeds as an environmentally friendly coagulant: Laboratory and pilot plant studies. *Journal of Chemical Technology & Biotechnology, 81*(12), 1852–1858. https://doi.org/10.1002/jctb.1619

Bhutada, P. R., Jadhav, A. J., Pinjari, D. V., Nemade, P. R., & Jain, R. D. (2016). Solvent assisted extraction of oil from Moringa oleifera Lam. seeds. *Industrial Crops and Products, 82*, 74–80. https://doi.org/10.1016/j.indcrop.2015.12.004

Biswal, A. K., Chakraborty, S., Saha, J., Panda, P. K., Pradhan, S. K., Behera, P. K., et al. (2024). Process Optimization, fabrication, and characterization of a starch-based biodegradable film derived from an underutilized crop. *ACS Food Science & Technology, 4*(8), 1844–1863. https://doi.org/10.1021/acsfoodscitech.4c00149

Cai, W.-Q., Liu, X., Chen, W., Huang, Z., Li, C., Huang, X., et al. (2023). Synergistic effect of lecithin and alginate, CMC, or PVP in stabilizing curcumin and its potential mechanism. *Food Chemistry, 413*, 1–11. https://doi.org/10.1016/j.foodchem.2023.135634

Celebioglu, A., Topuz, F., Irem Yildiz, Z., & Uyar, T. (2019). *Efficient removal of polycyclic aromatic hydrocarbons and heavy metals from water by electrospun nanofibrous polycyclodextrin membranes*. https://doi.org/10.1021/acsomega.9b00279.

Chowdhury, S., & Saha, P. Das (2011). Biosorption kinetics, thermodynamics and isosteric heat of sorption of Cu(II) onto Tamarindus indica seed powder. *Colloids and Surfaces B: Biointerfaces, 88*(2), 697–705. https://doi.org/10.1016/j.colsurfb.2011.08.003

Coldebella, P. F., Valverde, K. C., Yamaguchi, N. U., Ferreira, M. E. C., Camacho, F. P., & Silva, M. F. (2024). Exploring the eco-friendly potential of Moringa oleifera parts as biosorbents for atrazine removal. *International Journal of Environmental Science and Technology, 21*(9), 6445–6458. https://doi.org/10.1007/s13762-024-05462-6

Darwesh, H., Mohamed, R. R., & Soliman, S. M. A. (2024). Synthesis of novel antibacterial grafted sodium alginate copolymer-based adsorbent for wastewater treatment. *Polymer Bulletin, 81*(2), 1675–1689. https://doi.org/10.1007/s00289-023-04754-0

Dash, S., Gutti, P., Behera, B., & Mishra, D. (2024). Anionic species from multivalent metal salts are differentially retained during aqueous ionic gelation of sodium alginate and could fine-tune the hydrogel properties. *International Journal of Biological Macromolecules, 265*, 2478–2488. https://doi.org/10.1016/j.ijbiomac.2024.130767

Dehnad, D., Ghorani, B., Emadzadeh, B., Zhang, F., Yang, N., & Jafari, S. M. (2024). Electrospinning of legume proteins: Fundamentals, fiber production, characterization, and applications with a focus on soy proteins. *Food Hydrocolloids, 151*, 1–16. https://doi.org/10.1016/j.foodhyd.2024.109795

Dodero, A., Alloisio, M., Vicini, S., & Castellano, M. (2020). Preparation of composite alginate-based electrospun membranes loaded with ZnO nanoparticles. *Carbohydrate Polymers, 227*, 1–8. https://doi.org/10.1016/J.CARBPOL.2019.115371

Dos Santos Paglione, I., Galindo, M. V., de Medeiros, J. A. S., Yamashita, F., Alvim, I. D., & Ferreira Grosso, C. R. (2019). Comparative study of the properties of soy protein concentrate films containing free and encapsulated oregano essential oil. *Food Packaging and Shelf Life, 22*, 2–8. https://doi.org/10.1016/j.fpsl.2019.100419

Elkhatib, E. A., Mahdy, A. M., & Salama, K. A. (2015). Green synthesis of nanoparticles by milling residues of water treatment. *Environmental Chemistry Letters, 13*(3), 333–339. https://doi.org/10.1007/s10311-015-0506-6

Elo, T., Parihar, V. S., Bera, A., Javanshour, F., Kellomäki, M., & Layek, R. (2024). Mechanically robust, transparent, and UV-shielding composite of Na-Alginate and maleic acid-functionalized boron nitride nanosheets with improved antioxidant property. *Colloids and Surfaces B: Biointerfaces, 233*, 1–9. https://doi.org/10.1016/j.colsurfb.2023.113641

Freitas, E. D., Vidart, J. M. M., da Silva, M. G. C., & Vieira, M. G. A. (2021). Thermal characterization and stability investigation of sericin and alginate blend loaded with diclofenac sodium or ibuprofen. *European Polymer Journal, 142*, 1–10. https://doi.org/10.1016/j.eurpolymj.2020.110125

Fu, X., Su, J., Hou, L., Zhu, P., Hou, Y., Zhang, K., et al. (2021). Physicochemical and thermal characteristics of Moringa oleifera seed oil. *Advanced Composites and Hybrid Materials, 4*(3), 685–695. https://doi.org/10.1007/s42114-021-00302-4

Gharsallah, K., Rezig, L., Rajoka, M. S. R., Mehwish, H. M., Ali, M. A., & Chew, S. C. (2023). Moringa oleifera: Processing, phytochemical composition, and industrial applications. *South African Journal of Botany, 160*, 180–193. https://doi.org/10.1016/j.sajb.2023.07.008

Gomes, H., de, O., Freire, P., de, T. C., do Nascimento, R. F., & Pereira Teixeira, R. N. (2022). Removal of contaminants from water using Moringa oleifera Lam. as biosorbent: An overview of the last decade. *Journal of Water Process Engineering, 46*, 1–14. https://doi.org/10.1016/j.jwpe.2022.102576

Gopalakrishnan, L., Doriya, K., & Kumar, D. S. (2016). Moringa oleifera: A review on nutritive importance and its medicinal application. *Food Science and Human Wellness, 5*(2), 49–56. https://doi.org/10.1016/j.fshw.2016.04.001

Gover Antoniraj, M., Maria Leena, M., Moses, J. A., & Anandharamakrishnan, C. (2020). Cross-linked chitosan microparticles preparation by modified three fluid nozzle spray drying approach. *International Journal of Biological Macromolecules, 147*, 1268–1277. https://doi.org/10.1016/j.ijbiomac.2019.09.254

Hamadeen, H. M., Elkhatib, E. A., Badawy, M. E. I., & Abdelgaleil, S. A. M. (2021). Green low cost nanomaterial produced from Moringa oleifera seed waste for enhanced removal of chlorpyrifos from wastewater: Mechanism and sorption studies. *Journal of Environmental Chemical Engineering, 9*(4), 1–14. https://doi.org/10.1016/j.jece.2021.105376

He, Y., Du, E., Zhou, X., Zhou, J., He, Y., Ye, Y., et al. (2020). Wet-spinning of fluorescent fibers based on gold nanoclusters-loaded alginate for sensing of heavy metal ions and anti-counterfeiting. *Spectrochimica Acta Part A: Molecular and Biomolecular Spectroscopy, 230*, 1–10. https://doi.org/10.1016/j.saa.2020.118031

He, Y., Zhang, N., Gong, Q., Qiu, H., Wang, W., Liu, Y., et al. (2012). Alginate/graphene oxide fibers with enhanced mechanical strength prepared by wet spinning. *Carbohydrate Polymers, 88*(3), 1100–1108. https://doi.org/10.1016/j.carbpol.2012.01.071

Hu, X., Rajendran, S., Yao, Y., Liu, Z., Gopalsamy, K., Peng, L., et al. (2016). A novel wet-spinning method of manufacturing continuous bio-inspired composites based on graphene oxide and sodium alginate. *Nano Research, 9*(3), 735–744. https://doi.org/10.1007/s12274-015-0952-2

Hua, S., Ma, H., Li, X., Yang, H., & Wang, A. (2010). pH-sensitive sodium alginate/poly (vinyl alcohol) hydrogel beads prepared by combined Ca2+ crosslinking and freeze-thawing cycles for controlled release of diclofenac sodium. *International Journal of Biological Macromolecules, 46*(5), 517–523. https://doi.org/10.1016/j.ijbiomac.2010.03.004

Huang, X., Liang, K., Liu, Q., Qiu, J., Wang, J., & Zhu, H. (2020). Superfine grinding affects physicochemical, thermal and structural properties of Moringa Oleifera leaf powders. *Industrial Crops and Products, 151*, 1–7. https://doi.org/10.1016/j.indcrop.2020.112472

Hublikar, L. V., Shilar, F. A., Suliphuldevara Mathada, B., & Ganachari, S. V. (2024). A comprehensive investigation of green solutions for sustainable wastewater remediation: A review. *Journal of Molecular Liquids, 400*, 1–29. https://doi.org/10.1016/j.molliq.2024.124532

Hufenus, R., Yan, Y., Dauner, M., & Kikutani, T. (2020). Melt-spun fibers for textile applications. *Materials, 13*(19), 1–32. https://doi.org/10.3390/ma13194298

Hurtado, A., Aljabali, A. A. A., Mishra, V., Tambuwala, M. M., & Serrano-Aroca, Á. (2022). Alginate: enhancement strategies for advanced applications. *International Journal of Molecular Sciences, 23*(9), 1–45. https://doi.org/10.3390/ijms23094486

Jadbabaei, S., Kolahdoozan, M., Naeimi, F., & Ebadi-Dehaghani, H. (2021). Preparation and characterization of sodium alginate–PVA polymeric scaffolds by electrospinning method for skin tissue engineering applications. *RSC Advances, 11*(49), 30674–30688. https://doi.org/10.1039/D1RA04176B

Jafari, H., Ghaffari-bohlouli, P., Podstawczyk, D., Nie, L., & Shavandi, A. (2022). Tannic acid post-treatment of enzymatically crosslinked chitosan-alginate hydrogels for biomedical applications. *Carbohydrate Polymers, 295*, 1–13. https://doi.org/10.1016/j.carbpol.2022.119844

Jiang, W., Xiang, W., Lu, W., Yuan, D., Gao, Z., Hu, B., et al. (2023). Emulsifying performance of the hexadecyltrimethylammonium bromide (CTAB) complexed alginate microgels: Effects from their deformability on oil-water interface. *International Journal of Biological Macromolecules, 253*, 1–9. https://doi.org/10.1016/j.ijbiomac.2023.127509

Kalyani, S., Smitha, B., Sridhar, S., & Krishnaiah, A. (2006). Separation of ethanol−water mixtures by pervaporation using sodium alginate/poly(vinyl pyrrolidone) blend membrane crosslinked with phosphoric acid. *Industrial & Engineering Chemistry Research, 45*(26), 9088–9095. https://doi.org/10.1021/ie060085y

Kebede, T., Dube, S., & Express, M. N.-M. R. (2018). Fabrication and characterization of electrospun nanofibers from Moringa stenopetala seed protein. *Iopscience.Iop.Org, 5*, 1–12. https://iopscience.iop.org/article/10.1088/2053-1591/aae04c/meta.

Kebede, T. G., Mengistie, A. A., Dube, S., Nkambule, T. T. I., & Nindi, M. M. (2018). Study on adsorption of some common metal ions present in industrial effluents by Moringa stenopetala seed powder. *Journal of Environmental Chemical Engineering, 6*(1), 1378–1389. https://doi.org/10.1016/j.jece.2018.01.012

Kolanthai, E., Sindu, P. A., Khajuria, D. K., Veerla, S. C., Kuppuswamy, D., & Catalani, L. H. (2018). Graphene oxide—A tool for the preparation of chemically crosslinking free alginate–chitosan–collagen scaffolds for bone tissue engineering. *ACS Applied Materials & Interfaces, 10*(15), 12441–12452. https://doi.org/10.1021/acsami.8b00699

Kouadio, Olivier Kouadio, Yapi, Elisée Kouakoua, Kouadio, Claver Degbeu, Vladmir, Gbocho, & N'guessan, Georges Amani (2024). Effect of drying type on the physicochemical and phytochemical properties of young and mature Moringa oleifera leaves. *World Journal of Advanced Research and Reviews, 21*(2), 1000–1106. https://doi.org/10.30574/wjarr.2024.21.2.0296

Kumar, B., Singh, N., & Kumar, P. (2024). A review on sources, modification techniques, properties and potential applications of alginate-based modified polymers. *European Polymer Journal, 213*, 1–25. https://doi.org/10.1016/j.eurpolymj.2024.113078

Leone, A., Spada, A., Battezzati, A., Schiraldi, A., Aristil, J., & Bertoli, S. (2015). Cultivation, genetic, ethnopharmacology, phytochemistry and pharmacology of moringa oleifera leaves: an overview. *International Journal of Molecular Sciences, 16*(12), 12791–12835. https://doi.org/10.3390/ijms160612791

Li, Y., Wu, Y., Zhai, H., Qiao, C., Zhao, G., Xue, Z., et al. (2024). Effect of the pre-crosslinking of Ba2+ ions on wet spinning of agar fibers. *International Journal of Biological Macromolecules, 259*, 1–8. https://doi.org/10.1016/j.ijbiomac.2023.129169

Liao, Y., Loh, C. H., Tian, M., Wang, R., & Fane, A. G. (2018). Progress in electrospun polymeric nanofibrous membranes for water treatment: Fabrication, modification and applications. In *Progress in polymer science,, 77,* pp. 69–94). https://doi.org/10.1016/j.progpolymsci.2017.10.003

Lin, S. C.-Y., Wang, Y., Wertheim, D. F., & Coombes, A. G. A. (2017). Production and in vitro evaluation of macroporous, cell-encapsulating alginate fibres for nerve repair. *Materials Science and Engineering: C, 73*, 653–664. https://doi.org/10.1016/j.msec.2016.12.016

Luckachan, G. E., & Pillai, C. K. S. (2011). Biodegradable polymers- a review on recent trends and emerging perspectives. *Journal of Polymers and the Environment, 19*(3), 637–676. https://doi.org/10.1007/s10924-011-0317-1

Madala, S., Nadavala, S. K., Vudagandla, S., Boddu, V. M., & Abburi, K. (2017). Equilibrium, kinetics and thermodynamics of Cadmium (II) biosorption on to composite chitosan biosorbent. *Arabian Journal of Chemistry, 10*, S1883–S1893. https://doi.org/10.1016/j.arabjc.2013.07.017

Magalhães Souza, P., Bellanda Galuch, M., Lopes, A. P., Santos Pizzo, J., Campos Castro, M., & Maldonado Cruz, V. H. (2022). Assessment of moringa oleifera lam. seeds potential as an adsorbent material for soybean oil bleaching. *Revista Virtual de Química, 14*(2), 258–266. https://doi.org/10.21577/1984-6835.20220006

Marsano, E., Corsini, P., Arosio, C., Boschi, A., Mormino, M., & Freddi, G. (2005). Wet spinning of Bombyx mori silk fibroin dissolved in N-methyl morpholine N-oxide and properties of regenerated fibres. *International Journal of Biological Macromolecules, 37*(4), 179–188. https://doi.org/10.1016/j.ijbiomac.2005.10.005

Masitlha, E. P., Seifu, E., & Teketay, D. (2024). Nutritional composition and mineral profile of leaves of Moringa oleifera provenances grown in Gaborone, Botswana. *Food Production, Processing and Nutrition, 6*(1), 1–9. https://doi.org/10.1186/s43014-023-00183-8

Mehwish, H. M., Rajoka, M. S. R., Xiong, Y., Cai, H., Aadil, R. M., Mahmood, Q., et al. (2021). Green synthesis of a silver nanoparticle using Moringa oleifera seed and its applications for antimicrobial and sun-light mediated photocatalytic water detoxification. *Journal of Environmental Chemical Engineering, 9*(4), 1–13. https://doi.org/10.1016/j.jece.2021.105290

Militao, I. M., Roddick, F., Bergamasco, R., & Fan, L. (2022). Rapid adsorption of PFAS: Application of Moringa oleifera seed powder encapsulated in alginate beads. *Environmental Technology & Innovation, 28*, 1–13. https://doi.org/10.1016/J.ETI.2022.102761

Mishra, G., & Panda, P. K. (2024). Impact of surfactants on SWCNT dispersion in N-methylmorpholine N-Oxide for cellulose dissolution. *Journal of the Indian Chemical Society, 101*(8), 1–6. https://doi.org/10.1016/j.jics.2024.101210

Mishra, K., & Sinha, S. (2023). Biodegradable green composite film developed from Moringa Oleifera (Sahajana) seed filler and PVA: Surface functionalization, characterization and barrier properties. *Journal of Thermoplastic Composite Materials, 36*(1), 345–371. https://doi.org/10.1177/08927057211007550

Orisawayi, A. O., Koziol, K., Hao, S., Tiwari, S., & Rahatekar, S. S. (2024). Development of hybrid electrospun alginate-pulverized moringa composites. *RSC Advances, 14*(12), 1–11. https://doi.org/10.1039/D4RA00162A

Ortolá, M. D., Pageo, S., García-Mares, F. J., Juan-Borrás, M., & Castelló, M. L. (2024). Characterization of partially defatted moringa seed flour obtained at different temperatures. *LWT, 198*, 1–8. https://doi.org/10.1016/j.lwt.2024.115901

Panda, P. K., Sadeghi, K., & Seo, J. (2022). Recent advances in poly (vinyl alcohol)/natural polymer based films for food packaging applications: A review. *Food Packaging and Shelf Life, 33*, 1–13. https://doi.org/10.1016/j.fpsl.2022.100904

Park, J.-S., Park, C.-W., Han, S.-Y., Lee, E.-A., Cindradewi, A., Kim, J.-K., et al. (2021). Preparation and properties of wet-spun microcomposite filaments from various CNFs and alginate. *Polymers, 13*(11), 1–11. https://doi.org/10.3390/polym13111709

Pawar, S. N., & Edgar, K. J. (2012). Alginate derivatization: A review of chemistry, properties and applications. *Biomaterials, 33*(11), 3279–3305. https://doi.org/10.1016/j.biomaterials.2012.01.007

Popa, M. I., Lisa, G., & Aelenei, N. (2008). Thermogravimetric characterization of chitosan/alginate microparticles loaded with different drugs. *Polymer Bulletin, 61*(4), 481–490. https://doi.org/10.1007/s00289-008-0973-z

Qin, Y., Jiang, J., & Wang, F. (2018). Applications of alginate as a functional food ingredient. In A. M. Grumezescu, & A. M. Holban (Eds.), *Biopolymers for Food Design* (pp. 409–429). Academic Press, Elsevier. doi.org/10.1016/B978-0-12-811449-0.00013-X.

Ramdhan, T., Ching, S. H., Prakash, S., & Bhandari, B. (2020). Physical and mechanical properties of alginate based composite gels. *Trends in Food Science and Technology, 106*, 150–159. https://doi.org/10.1016/j.tifs.2020.10.002

Ravikumar, U., & Mater, J. (2020). Moringa oleifera seed composite a novel material for hazardous heavy metals (Cd, Cr and Pb) removal from aqueous systems. *J. Mater. Environ. Sci, 2020*(1), 123–138. http://www.jmaterenvironsci.com.

Safaei, M., & Moghadam, A. (2022). Optimization of the synthesis of novel alginate-manganese oxide bionanocomposite by Taguchi design as antimicrobial dental impression material. *Materials Today Communications, 31*, 1–9. https://doi.org/10.1016/j.mtcomm.2022.103698

Saha, P., & Paul, B. (2019). Assessment of heavy metal toxicity related with human health risk in the surface water of an industrialized area by a novel technique. *Human and Ecological Risk Assessment: An International Journal, 25*(4), 966–987. https://doi.org/10.1080/10807039.2018.1458595

Sahoo, D. R., & Biswal, T. (2021). Alginate and its application to tissue engineering. *SN Applied Sciences, 3*(1), 1–19. https://doi.org/10.1007/s42452-020-04096-w

Sampath, P., & Santhanam, S. K. V. (2019). Effect of moringa and bagasse ash filler particles on basalt/epoxy composites. *Polímeros, 29*(3), 1–7. https://doi.org/10.1590/0104-1428.01219

Santos, T. M., de Jesus, F. A., da Silva, G. F., & Pontes, L. A. M. (2020). Synthesis of activated carbon from oleifera moringa for removal of oils and greases from the produced water. *Environmental Nanotechnology, Monitoring & Management, 14*, 1–8. https://doi.org/10.1016/j.enmm.2020.100357

Sattariazar, S., Nejad Ebrahimi, S., & Arsalani, N. (2023). Enhancing the properties of electrospun polyvinyl Alcohol/Oxidized sodium alginate nanofibers with fluorescence carbon Dots: Preparation and characterization. *International Journal of Pharmaceutics, 644*, 1–9. https://doi.org/10.1016/j.ijpharm.2023.123358

Savitha, S., Surendhiran, S., Balu, K. S., & Karthik, A. (2024). In-vitro and bio-electrochemical characteristics of phytochemical enriched Co_3O_4 nanoparticles loaded biomimetic scaffold for preclinical analysis. *Polymers for Advanced Technologies, 35*(1), 1–17. https://doi.org/10.1002/pat.6215

Sibaja, B., Culbertson, E., Marshall, P., Boy, R., Broughton, R. M., & Solano, A. A. (2015). Preparation of alginate–chitosan fibers with potential biomedical applications. *Carbohydrate Polymers, 134*, 598–608. https://doi.org/10.1016/j.carbpol.2015.07.076

Sideek, S. A., El-Nassan, H. B., Fares, A. R., Elkasabgy, N. A., & ElMeshad, A. N. (2024). Cross-linked alginate dialdehyde/chitosan hydrogel encompassing curcumin-loaded bilosomes for enhanced wound healing activity. *Pharmaceutics, 16*(1), 1–30. https://doi.org/10.3390/pharmaceutics16010090

Susanto, H., Wonorahardjo, S., Putra, W. E., Taufiq, A., Sunaryono, S., & Fadhilah, D. N. (2023). Phytochemical profiling and pharmaceutical properties of moringa oleifera leaves powder and seed oil against hepatocellular carcinoma. *Malaysian Journal of Fundamental and Applied Sciences, 19*(4), 691–706. https://doi.org/10.11113/mjfas.v19n4.2818

Tang, Z., Jia, S., Wang, F., Bian, C., Chen, Y., & Wang, Y. (2018). Highly stretchable core–sheath fibers via wet-spinning for wearable strain sensors. *ACS Applied Materials & Interfaces, 10*(7), 6624–6635. https://doi.org/10.1021/acsami.7b18677

Ureña-Benavides, E. E., Brown, P. J., & Kitchens, C. L. (2010). Effect of Jet stretch and particle load on cellulose nanocrystal−alginate nanocomposite fibers. *Langmuir : the ACS journal of surfaces and colloids, 26*(17), 14263–14270. https://doi.org/10.1021/la102216v

Vardhan, K. H., Kumar, P. S., & Panda, R. C. (2019). A review on heavy metal pollution, toxicity and remedial measures: Current trends and future perspectives. *Journal of Molecular Liquids, 290*, 1–22. https://doi.org/10.1016/j.molliq.2019.111197

Varughese, S. A., Gokul, S., & Keerthi, P. (2024). Extraction of microfibrillated cellulose from elephant egesta and evaluating its reinforcing ability in pectin/alginate packaging films. *Polymer Composites, 45*(1), 680–694. https://doi.org/10.1002/pc.27807

Vázquez-Guerrero, A., Cortés-Martínez, R., Alfaro-Cuevas-Villanueva, R., Rivera-Muñoz, E., & Huirache-Acuña, R. (2021). Cd(II) and Pb(II) adsorption using a composite obtained from Moringa oleifera lam. cellulose nanofibrils impregnated with iron nanoparticles. *Water, 13*(1), 1–28. https://doi.org/10.3390/w13010089

Verdi, A. G., de Souza, A. G., Rocha, D. B., de Oliveira, S. A., Alves, R. M. V., & dos Santos Rosa, D. (2021). Biodegradable films functionalized with Moringa oleifera applied in food packaging. *Iranian Polymer Journal, 30*(3), 235–246. https://doi.org/10.1007/s13726-020-00885-7

Vincent, T., Vincent, C., Dumazert, L., Otazaghine, B., Sonnier, R., & Guibal, E. (2020). Fire behavior of innovative alginate foams. *Carbohydrate Polymers, 250*, 1–14. https://doi.org/10.1016/j.carbpol.2020.116910

Wade, S. J., Zuzic, A., Foroughi, J., Talebian, S., Aghmesheh, M., & Moulton, S. E. (2017). Preparation and in vitro assessment of wet-spun gemcitabine-loaded polymeric fibers: Towards localized drug delivery for the treatment of pancreatic cancer. *Pancreatology : official journal of the International Association of Pancreatology (IAP) ... [et al.], 17*(5), 795–804. https://doi.org/10.1016/j.pan.2017.06.001

Wang, J., Huang, X., Xiao, J., Yu, W., Wang, W., Xie, W., et al. (2010). Hydro-spinning: A novel technology for making alginate/chitosan fibrous scaffold. *Journal of Biomedical Materials Research Part A, 93A*(3), 910–919. https://doi.org/10.1002/jbm.a.32590

Wang, T., Liu, Y., Dong, J., Wang, Y., Li, D., Long, X., et al. (2024). Preparation of high-strength photochromic alginate fibers based on the study of flame-retardant properties. *International Journal of Biological Macromolecules, 258*, 1–9. https://doi.org/10.1016/j.ijbiomac.2023.128889

Watthanaphanit, A., Supaphol, P., Tamura, H., Tokura, S., & Rujiravanit, R. (2010). Wet-spun alginate/chitosan whiskers nanocomposite fibers: Preparation, characterization and release characteristic of the whiskers. *Carbohydrate Polymers, 79*(3), 738–746. https://doi.org/10.1016/j.carbpol.2009.09.031

Weatherbee-Martin, N., Xu, L., Hupe, A., Kreplak, L., Fudge, D. S., Liu, X.-Q., et al. (2016). Identification of wet-spinning and post-spin stretching methods amenable to recombinant spider aciniform silk. *Biomacromolecules, 17*(8), 2737–2746. https://doi.org/10.1021/acs.biomac.6b00857

Wu, Z., Chen, S., Li, J., Wang, B., Jin, M., Liang, Q., et al. (2023). Insights into hierarchical structure–property–application relationships of advanced bacterial cellulose materials. *Advanced Functional Materials, 33*(12), 1–32. https://doi.org/10.1002/adfm.202214327

Xu, J., Cao, Z., Zhang, Y., Yuan, Z., Lou, Z., Xu, X., et al. (2018). A review of functionalized carbon nanotubes and graphene for heavy metal adsorption from water: Preparation, application, and mechanism. *Chemosphere, 195*, 351–364. https://doi.org/10.1016/j.chemosphere.2017.12.061

Yadav, M., Rhee, K. Y., & Park, S. J. (2014). Synthesis and characterization of graphene oxide/carboxymethylcellulose/alginate composite blend films. *Carbohydrate Polymers, 110*, 18–25. https://doi.org/10.1016/j.carbpol.2014.03.037

Yang, J., Panda, P. K., Jie, C. J., Dash, P., & Chang, Y. (2022). Poly (vinyl alcohol)/chitosan/sodium alginate composite blended membrane: Preparation, characterization, and water-induced shape memory phenomenon. *Polymer Engineering & Science, 62*(5), 1526–1537. https://doi.org/10.1002/pen.25941

Yao, Y., Allardyce, B. J., Rajkhowa, R., Hegh, D., Qin, S., Usman, K. A. S., et al. (2022). Toughening wet-spun silk fibers by silk nanofiber templating. *Macromolecular Rapid Communications, 43*(7), 1–9. https://doi.org/10.1002/marc.202100891

Zhang, Z., Kong, Y., Gao, J., Han, X., Lian, Z., Liu, J., et al. (2024). Engineering strong man-made cellulosic fibers: A review of the wet spinning process based on cellulose nanofibrils. *Nanoscale, 6*(3), 6383–6401. https://doi.org/10.1039/D3NR06126D

Zhang, Z.-H., Chen, Z.-Y., Tang, Y.-H., Li, Y.-T., Ma, D., Zhang, G.-D., et al. (2022). Silicone/graphene oxide co-cross-linked aerogels with wide-temperature mechanical flexibility, super-hydrophobicity and flame resistance for exceptional thermal insulation and oil/water separation. *Journal of Materials Science & Technology, 114*, 131–142. https://doi.org/10.1016/j.jmst.2021.11.012

Zhao, X., Zhu, H., Chen, J., & Ao, Q. (2015). FTIR, XRD and SEM analysis of ginger powders with different size. *Journal of Food Processing and Preservation, 39*(6), 2017–2026. https://doi.org/10.1111/jfpp.12442



https://dspace.org/

Development and characterisation of integrated wet-spun alginate-Moringa oleifera composite fibers for potential water purification

Orisawayi, Abimbola Oluwatayo; Koziol, Krzysztof K.; Rahatekar, Sameer S.

2025-03
Elsevier
https://doi.org/10.1016/j.carpta.2024.100620
Orisawayi AO, Koziol K, Rahatekar SS. (2025) Development and characterisation of integrated wet-spun alginate-Moringa oleifera composite fibers for potential water purification. Carbohydrate Polymer Technologies and Applications, Volume 9, March 2025, Article number 100620

Downloaded from a DSpace repository. https://dspace.org/